Journal of Nuclear Materials 555 (2021) 153138

Contents lists available at ScienceDirect

Journal of Nuclear Materials

journal homepage: www.elsevier.com/locate/jnucmat

Review

Spent nuclear fuel in dry storage conditions – current trends in fuel performance modeling

Piotr Konarski*, Cédric Cozzo, Grigori Khvostov, Hakim Ferroukhi

Paul Scherrer Institut (PSI), Nuclear Energy and Safety Department, Forschungsstrasse 111, Villigen 5232, Switzerland

ARTICLE INFO

Article history:
Received 20 January 2021
Revised 4 June 2021
Accepted 7 June 2021
Available online 23 June 2021

Keywords:
Dry storage
Spent nuclear fuel
Fuel performance modeling
Delayed hydride cracking
Hydride reorientation
Long-term creep

ABSTRACT

The role of dry storage in spent nuclear fuel management becomes more and more important. Originally intended to serve as a temporary solution for a few decades until final disposal, now dry storage period is to be extended to 100 years and beyond. It has to be proven for licensing that the fuel rod integrity during dry storage is ensured. Since it is difficult to provide experimental support, the licensing process has to rely largely on numerical simulations. This paper reviews the literature associated with the modeling of spent nuclear fuel under dry storage conditions. The main phenomena threatening the fuel rod integrity and the numerical models representing them are described here. Moreover, the most recent or currently ongoing experimental efforts that could support the modeling of nuclear fuel in dry storage in the future are discussed. Finally, this paper reviews approaches to dry storage modeling chosen by different countries. In general, these approaches are similar and can be described as a calculation chain consisting of neutronics–thermo-hydraulics–fuel performance computations where sensitivity and uncertainty studies are crucial elements.

1. Introduction

After discharge from the reactor, hot and highly radioactive Spent Nuclear Fuel (SNF) is moved for wet storage to an on-site pool until its decay heat is sufficiently low for further storing options. However, limited capacities of such pools drive development of strategies for interim storage of SNF in out-of-site repositories until final disposal. Currently, the two options are wet and dry storage. However, the latter one receives more attention for several reasons: dry storage solutions are mature, ready-to-implement and rely on passive safety principles. In addition, dry storage facilities can be easily expanded to accommodate more fuel. Another advantage of this storage option is cost efficiency over a long period and possibility of direct transportation of the dual purpose (transport and storage) casks to a final repository site.

Dry storage has been chosen as an interim storage method in many countries including Canada, Germany, Switzerland and the U.S[1]. Also, it gets more attention in countries like China, Russia and Korea. Dry storage was also studied in France in the framework of the PRECCI project [2]. As dry storage is a temporary solution for SNF management, it has been licensed for a limited period of time. Initially, proposed storage periods were between 20 and 50 years, depending on the country. Since the projects of final repositories around the world are generally delayed due to issues with licensing and social acceptance, the interim storage period needs to be extended.

Fuel rod integrity during extended dry storage has to be ensured until final disposal. Current trends are to extend the interim storage period to around 100 years or even beyond. In this time frame, safety assessment needs to be based on experimental observations and supported by numerical tools. Decades of development of fuel performance codes allow to explain and predict different types of fuel behavior during both normal reactor operation and accidents [3]. However, modeling of the fuel behavior in dry storage conditions had little attention up to now. Typical dry storage conditions, described in Section 2, are different compared to reactor operation. Experimental and numerical efforts aimed at studying long time effects, relevant to dry storage, like the cladding creep or hydrogen behavior are limited. Section 3 gives a brief description of the models and correlations that can be applied to dry storage simulations.

New models anticipating the rod behavior in dry storage will be developed in the future thanks to ongoing experiments like these at the Kurchatov Institute in Russia [4] or Paul Scherrer Institute (PSI) in Switzerland [5,6]. Recent experiments and planned programs are discussed in Section 4.

Growing needs for numerical analyses concern not only fuel performance modeling but also other aspects of dry storage.

* Corresponding author.
E-mail addresses: piotr.konarski@psi.ch (P. Konarski), cedric.cozzo@psi.ch (C. Cozzo).

https://doi.org/10.1016/j.jnucmat.2021.153138
0022-3115/

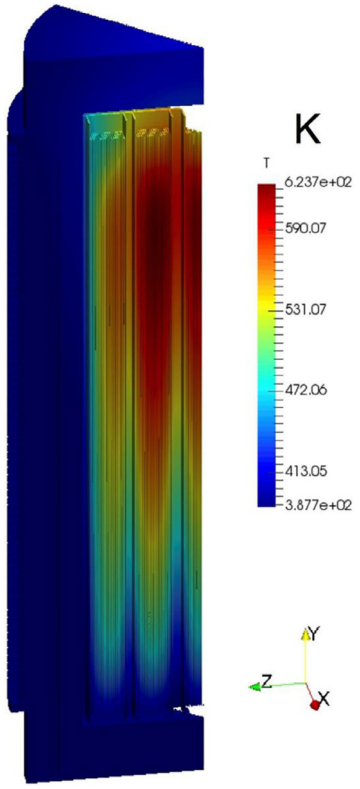

Fig. 1. Numerical prediction of the temperature distribution in a PWR storage cask. Note high temperature variations as a function of the axial position. A section of two and a half fuel assemblies can be seen. Figure from Arkoma et al. [15].

Numerous publications studying criticality, shielding, thermo-hydraulics or mechanics of dry storage casks are available [7–12]. Such simulations provide boundary conditions and their uncertainties for fuel behavior modeling. Therefore, these inter-dependencies need identification and detailed sensitivity and uncertainty studies. Such multiphysics calculations proposed by different countries are presented in Section 5.

2. Dry storage conditions

Before discussing phenomena important in dry storage, it is crucial to define what range of temperatures, pressures and hydrogen contents can be expected in dry storage.

2.1. Temperature

SNF reaches its maximum temperature at the end of drying which is a transition process between wet and dry storage. The drying can be done using different methods, for instance, vacuum drying or forced helium drying. According to the recommendations released by the U.S Nuclear Regulatory Commission (NRC), the cladding peak temperature should not exceed 400 °C [13]. However, a higher short-term temperature limit can be used for low burnup fuel (<45 GWd/tU) if the cladding hoop stress does not exceed 90 MPa. Much lower temperature limits have been proposed in Japan. According to the Japanese regulations, the maximum allowed cladding temperatures vary from 200 to 300 °C depending on the cladding type and burnup [14].

Another important aspect is the temperature axial profile within a cask. As can be seen in Fig. 1, the rod temperature at different elevations can be very different. It depends on many factors like the burnup, fuel type, position in storage cask and cask model itself. A general storing trend is to keep the rod plena at lower

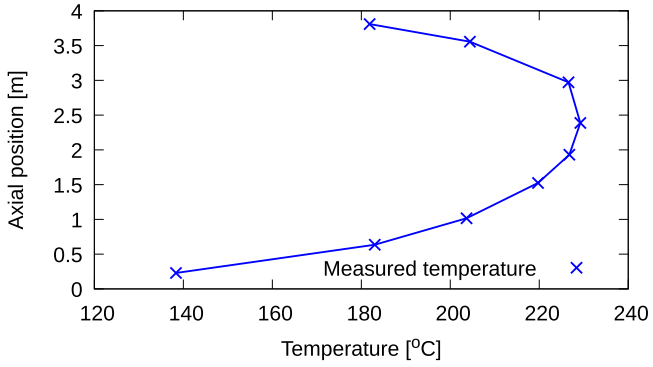

Fig. 2. Temperature axial profile measured near the cask center at the beginning of dry storage. Data provided by the Electric Power Research Institute EPRI [17].

temperatures because most of the rod internal gas is located there and its expansion would generate additional stress on the cladding.

The maximum temperature in Fig. 1 is close to the 400 °C limit proposed by NRC. However, in actual dry storage the expected temperatures are lower. Recently, a realistic temperature distribution in a cask has been obtained within the DEMO project [16]. In the frame of DEMO, high burnup fuel assemblies were loaded into a modified TN32 cask equipped with numerous thermocouples allowing to monitor temperature inside the cask at different axial and radial positions. An example of an axial temperature profile measured at the beginning of dry storage near the cask center is shown in Fig. 2. As can be seen, the maximum temperature is around 230 °C which is considerably lower than in Fig. 1. More details of DEMO are given in Section 4.5.

2.2. Rod internal pressure and cladding stresses

Manufactured PWR fuel rods are filled with helium up to 3.5 MPa at room temperature. The Rod Internal Pressure (RIP) increases during irradiation due to Fission Gas Release (FGR), fuel swelling etc. At high burnup, it can reach more than 6.5 MPa [18]. RIP can be several times higher than the dry storage cask pressure. This differential pressure is the source of the cladding stress during dry storage. Sufficiently high stress can lead to reorientation of hydrides.

As previously mentioned, the maximum allowed cladding hoop stress in the low burnup fuels in the U.S. is limited to 90 MPa if the temperature is higher than 400 °C [13]. In Japan, the limit stress allowed in dry storage varies between 70 and 100 MPa, depending on the cladding type [14].

2.3. Hydrogen concentration

Zr-based claddings undergo a slow corrosion process in reaction with the coolant water [19]:

$$Zr + 2H_2O \rightarrow ZrO_2 + 2H_2 \quad (1)$$

The fraction of the hydrogen produced in this reaction that enters the cladding is called the pickup fraction. The degree of oxidation, pickup fraction and concentration of the picked up hydrogen differ significantly depending on the cladding material, irradiation conditions and burnup. For instance, standard Zircaloy-4 claddings can reach the average hydrogen content as high as 600–700 wppm at the end of life; whereas modern, corrosion resistant materials like M5^{TM}, have the average hydrogen concentration around 100 wppm at the same burnup [20]. However, before the picked up hydrogen reaches the metal, it travels through the oxide layer ZrO_2 formed on the cladding outer wall. It has been recently proposed that the hydrogen transport towards the metal is driven by a force

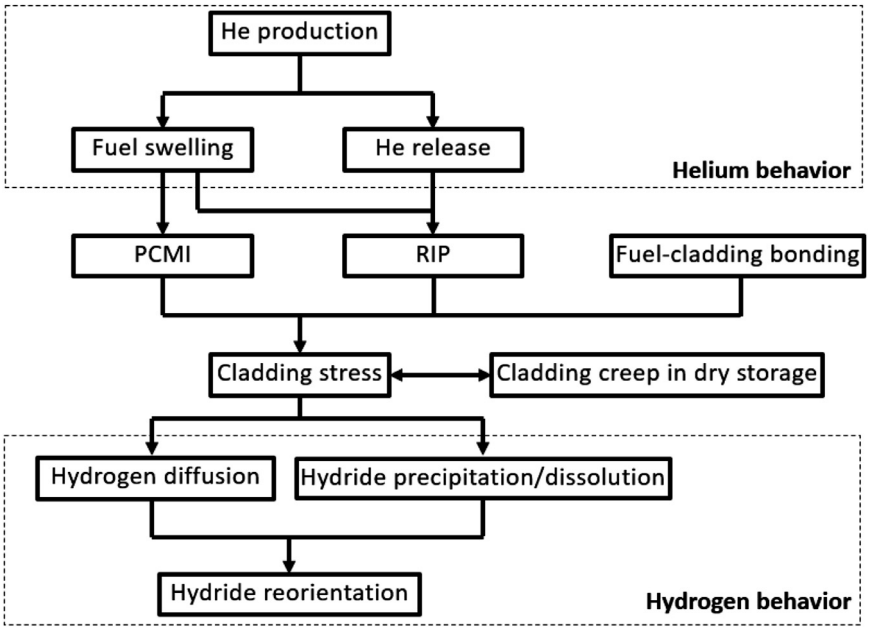

Fig. 3. A simplified scheme of the stress-related phenomena important in dry storage. PCMI stands for Pellet-Cladding Mechanical Interaction and RIP for Rod Internal Pressure.

inversely proportional to the electronic conductivity of the ZrO_2 layer [21]. The hydrogen migration mechanism in response to this driving force has not been determined yet but it is believed that the hydrogen migrates as H^+ [22–24]. Once the hydrogen reaches the metal, it can migrate driven by concentration, temperature and stress gradients. In non-liner claddings, it tends to move towards the outer cladding part where it precipitates and forms the so-called 'hydride rim' with the maximum hydrogen content exceeding 2000 wppm [20]. The precipitation of hydrogen is a consequence of its limited solubility in zirconium alloys. Once the maximum concentration of hydrogen at a given temperature is reached, hydrogen precipitates into hydrides. The solubility of hydrogen is explained in more detail in Section 3.5.1.

3. Important phenomena

According to the gap analyses done by NRC [25] and Department of Energy (DOE) [26], two possible degradation mechanisms of the fuel rod cladding are creep and Delayed Hydride Cracking (DHC). These phenomena can be driven high RIP causing tensile stresses in the cladding. The high internal pressure is a consequence of several phenomena. First, fission gas is created and released to the rod free volume during irradiation. Second, helium produced by α decays of actinides during operation and storage can also be released to the rod free volume and contribute to RIP. Moreover, α-decay damage results in the lattice parameter increase which is associated with fuel swelling [27,28]. Helium–induced fuel swelling can have important consequences in terms of the Pellet-Cladding Mechanical Interaction (PCMI). The distribution of stresses in the cladding can be also significantly affected by the pellet-cladding bonding if such a phenomenon, associated with high burnup fuel, occurs.

This section describes publications focused on modeling the stress-related phenomena as shown in Fig. 3. It accounts for both the phenomena contributing to the cladding stress like helium production and the phenomena being a consequence of it like creep or hydrogen redistribution. It is important to specify that Fig. 3 is simplified. It is focused on the stress-related effects to create a comprehensive chain of dependencies between the phenomena important in dry storage. However, other parameters like, for instance, temperature, cladding type or the presence of cladding liners are also important and cannot be neglected.

In addition, a paragraph in this section is dedicated to transportation of SNF, not mentioned in Fig. 3. During transportation, SNF is submitted to cyclic vibrations that may lead to fatigue failure. Even though this aspect has not been studied by the fuel performance community, it deserves attention because implementing mechanical fatigue correlations into fuel performance codes could improve their modeling capabilities.

3.1. Helium production and behavior

There are two main sources of helium in a spent fuel rod. First, helium is the filling gas in rod manufacture. The fill gas pressure depends on the rod design and it is higher in PWR than BWR fuel rods. Second, helium is produced via α decay of actinides, mostly Pu and Cm [29]. Helium production is much more significant in MOX fuel because of high abundance of actinides. Whereas the helium initially present in the fuel rod completely contributes to RIP, the helium generated from actinides can be responsible for two phenomena important in dry storage. Helium is either retained in the fuel matrix causing swelling, and potentially leading to PCMI, or released to the plenum and increasing RIP. Even if PCMI or high RIP do not lead directly to the failure, they affect the distribution of stress and its role in the hydrogen-related mechanisms in the cladding. According to the work done recently by Luzzi et al. [30] and Cognini et al. [31], the key parameters governing the behavior of helium in nuclear fuel are the helium diffusivity and solubility.

Apart from the two main sources of helium, it is worth to mention helium production in the Integral Fuel Burnable Absorber (IFBA) design from Westinghouse [32]. In this design, some fuel pellets in the assembly are covered with a thin layer of zirconium diboride. Helium is produced in consequence of the neutron absorption by ^{10}B and is released to plenum. The issues associated with IFBA are discussed in Section 3.2.3.

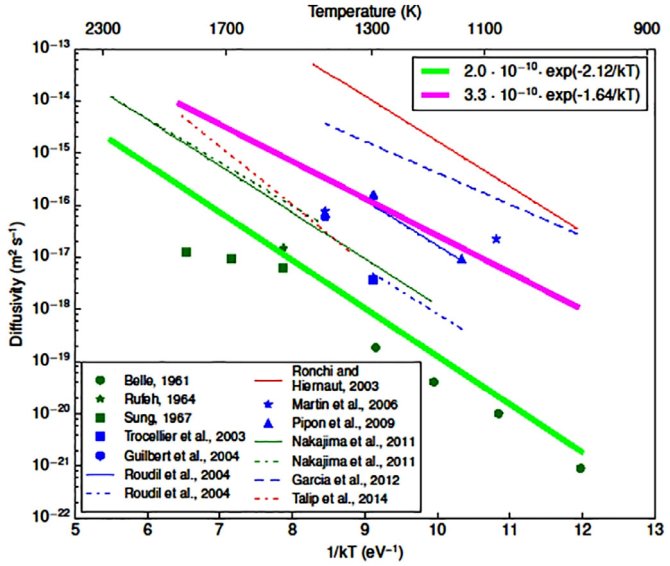

Fig. 4. Empirical correlations derived by Luzzi et al. (thick green and purple curves) compared to experimental data. Different colors indicate different helium implementation techniques. Dark green corresponds to infusion, blue to ion implementation and red to doping. Figure adapted from Luzzi et al. [30]. (For interpretation of the references to colour in this figure legend, the reader is referred to the web version of this article.)

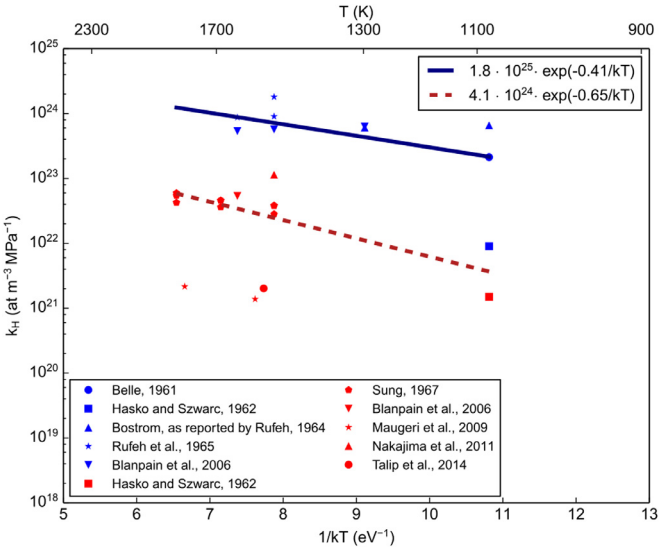

Fig. 5. Empirical correlations for helium solubility derived by Cognini et al. (curves) compared to experimental data (points). Different colors indicate different microstructure of the sample. Blue corresponds to powder samples red to single crystal samples. Figure from Cognini et al. [31]. (For interpretation of the references to colour in this figure legend, the reader is referred to the web version of this article.)

3.1.1. Helium diffusivity

Helium release strongly depends on the helium diffusion coefficient. A recent work of Luzzi et al. [30] gathers and analyzes the experimental studies on helium diffusivity. The authors reported that three main experimental techniques can be used to introduce helium in the samples. These are infusion, ionic implantation and doping. The two latter techniques cause damage to the lattice of the sample and create defects which result in fast helium diffusion. This observation is consistent with the enhanced diffusion of helium measured by Talip et al. in non-stoichiometric UO_2 [33].

Since the experimental method affects the obtained data, Luzzi et al. divided the experimental results into two groups depending on the helium introduction technique. The first group consists of the data obtained by infusion. In the second group, the authors placed the results obtained by ionic implementation and doping. Luzzi et al. used the data from both groups to fit two empirical correlations for the helium diffusion coefficient D_H. The correlation based on the first group is as follows:

$$D_H = 2.0 \times 10^{-10} \exp\left(-2.12/kT\right) \quad [\mathrm{m^2\ s^{-1}}] \tag{2}$$

where k [eV K^{-1}] is the Boltzmann constant and T [K] is temperature. Luzzi et al. recommended to use the above coefficient to model helium behavior in fresh fuel. For irradiated fuel, where a certain level of lattice damage is present, the authors suggested to use the function based on the second group of experimental data:

$$D_H = 3.3 \times 10^{-10} \exp\left(-1.64/kT\right) \quad [\mathrm{m^2\ s^{-1}}] \tag{3}$$

The comparison between the correlations obtained by Luzzi et al. and the experimental data is shown in Fig. 4. One can see that the experimental data used for the fitting is scattered and thus, empirical correlations are associated with high uncertainties. The authors estimated them to be of the order of a factor of ten for Eq. 2 and of a factor of one thousand for Eq. 3.

3.1.2. Helium solubility

The parameter governing helium retention is the helium solubility. Cognini et al. [31] have gathered and analyzed available experimental data concerning helium retention. In all of them, the infusion technique has been used to charge the samples with helium. It has been experimentally proven [34–36] that the helium solubility in UO_2 is proportional to the infusion pressure and obeys Henry's law given by:

$$C_s = k_H p \qquad [\mathrm{at\ m^{-3}}] \tag{4}$$

where p [MPa] is the infusion pressure and k_H [at m^{-3} MPa^{-1}] is the Henry's constant. According to Cognini et al., the helium solubility of the studied samples strongly depends on their microstructure. The powder samples are characterized by higher helium solubility than the single crystal samples as shown in Fig. 5. The authors have used the experimental data to derive empirical correlations describing the Henry's constant depending on microstructure. The correlation for the powder samples can be expressed as follows:

$$k_H = 1.8 \times 10^{25} \exp\left(-0.41/kT\right) \quad [\mathrm{at\ m^{-3}\ MPa^{-1}}] \tag{5}$$

where k [eV K^{-1}] is the Boltzmann constant and T [K] is temperature. According to Cognini et al., this correlation can be applied to study the helium behavior in the fuel after pulverization that can occur in LOCA. The function describing the Henry's constant in the single crystal samples is given by:

$$k_H = 4.1 \times 10^{24} \exp\left(-0.65/kT\right) \quad [\mathrm{at\ m^{-3}\ MPa^{-1}}] \tag{6}$$

The above equation can be used to analyze helium behavior at the grain scale. Some fission gas models used in fuel performance codes account for meso-scale phenomena. Examples of such models are GRSW-A [37] or a recent model developed by Verma et al. [38].

The Henry's law correlations derived by Cognini et al. have been compared to experimental measurements in Fig. 5. One can see that the prediction obtained by the authors has a good trend but the experimental data used for the fitting is significantly dispersed. Therefore, the empirical correlations are associated with high uncertainties of approximately one thousand.

3.1.3. Fuel pellet swelling

Fuel pellet swelling can be based on the helium solubility prediction described in the previous section. However, α decays of actinides in spent nuclear fuel can also cause swelling in a different way. Helium particles created by nuclear reactions knock on

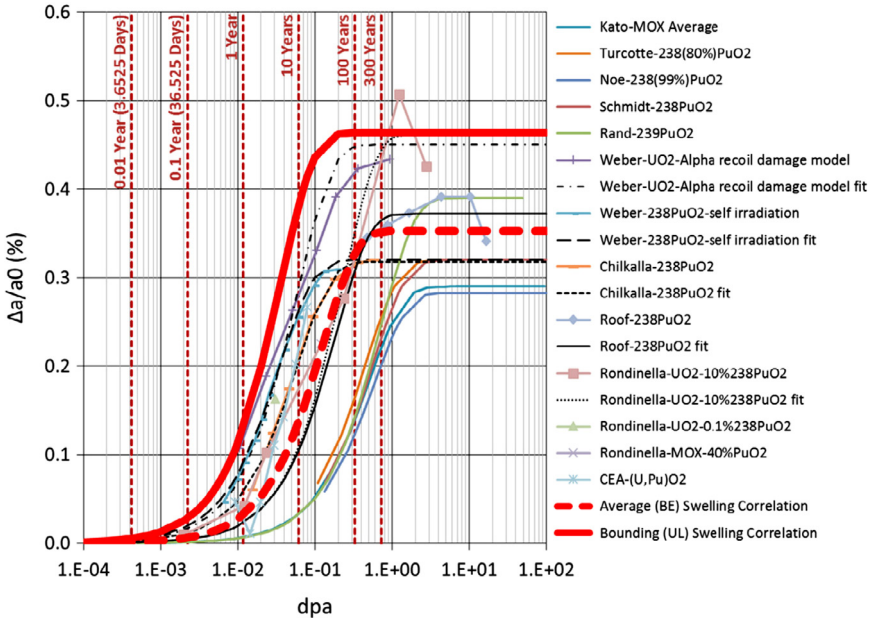

Fig. 6. Experimental data on fuel swelling compared to the correlations derived by Raynaud and Einziger (thick red curves). Figure from Raynaud and Einziger [28]. (For interpretation of the references to colour in this figure legend, the reader is referred to the web version of this article.)

atoms in the UO_2 lattice. Those interactions generate cascades of displacements resulting in lattice swelling. The literature regarding this phenomenon has been reviewed by Raynaud and Einziger [28]. The authors analyzed the gathered data and used them to derive the correlations describing the relative lattice expansion $\Delta a/a_0$ where a and a_0 are the deformed and undeformed lattice parameters as a function of dpa (displacements per atom). The best-estimate swelling correlation proposed by Raynaud and Einziger is as follows:

$$\frac{\Delta a}{a_0} = 3.528 \times 10^{-3}[1 - \exp(-8.492\ \text{dpa})] \tag{7}$$

Additionally, the authors reported the upper limit swelling correlation:

$$\frac{\Delta a}{a_0} = 4.642 \times 10^{-3}[1 - \exp(-28.077\ \text{dpa})] \tag{8}$$

The dpa used by Raynaud and Einziger in Eqs. 7 and 8 is based on the work of Rondinella et al.[27] and expressed as a function of time t:

$$\text{dpa}(t) = 1.1742 \times 10^{-2} \times t^{7.2246\times10^{-1}} \tag{9}$$

The results obtained by Raynaud and Einziger with Eqs. 7 and 8 are compared to the experimental data in Fig. 6.

3.2. Cladding stress

Helium-related effects described in previous sections can affect the cladding integrity either by increasing RIP (helium release) or by PCMI (fuel swelling). Both RIP and PCMI generate stresses in the cladding which can activate degradation mechanisms like creep, hydride reorientation or delayed hydride cracking.

3.2.1. NRC Analysis

Raynaud and Einziger from NRC have performed fuel performance simulations of several different BWR and PWR designs to study stresses in the cladding during dry storage [28,39]. The authors have used two different versions of the fuel code FRAPCON. FRAPCON-3.5 [40] has been utilized to predict fuel swelling and gas production whereas the modified version of FRAPCON-3.5, extended by adding the code DATING (Determine Allowable Temperatures in Inert and Nitrogen Gases) [41], has been employed to study cladding creep. The creep models available in DATING have been developed to model dry storage conditions, and thus they are more reliable that the creep laws available in FRAPCON-3.5.

The simulations carried out by the authors account for the base irradiation up to 65 GWd/tU, 5 years of wet storage and 295 years of dry storage. The temperature during wet storage remains close to 80 °C. At the beginning of dry storage the temperature rises up to 400 °C and decreases with time according to the relation:

$$T(K) = \begin{cases} 0.265714 \times t^2 - 12.3343 \times t + 673.15 & \text{if } t < 13.0306 \text{ years} \\ -59.2015 \times \ln(t) + 709.532 & \text{if } t \geq 13.0306 \text{ years} \end{cases} \tag{10}$$

In the FRAPCON-3.5 simulations, both fuel swelling correlations described in Section 3.1.3 have been used. The authors reported that the cladding stress obtained with the upper limit correlation (Eq. 8) is only slightly higher that the stress calculated with the best estimate correlation (Eq. 7). The calculated fuel swelling does not lead to gap closure during dry storage (gap opens at the beginning of wet storage) nor to PCMI in any of studied cases. However, it decreases the rod free volume and increases RIP.

RIP is also increased by the so-called decay gas. The decay gas is composed of H, He (main component), Kr, N, Ne, Ra and Xe produced during storage. Its concentration has been calculated with the code ORIGEN [42]. Its release during storage together with the initial helium filling and the FGR during base irradiation contribute to RIP. To investigate the impact of the decay gas release, Raynaud and Einziger have performed sensitivity studies. The authors assumed different fractions of the decay gas to be released to the rod free volume. An example of results obtained by Raynaud and Einziger for a PWR rod of a 17x17 design is shown in Fig. 7. The authors pointed out that the decay gas release fraction has to be greater than 20% to induce a stress increase during dry storage. If lower, it cannot compensate the RIP decrease caused by decreasing temperature. As seen in the right figure, the decay gas release does not affect the cladding strain significantly.

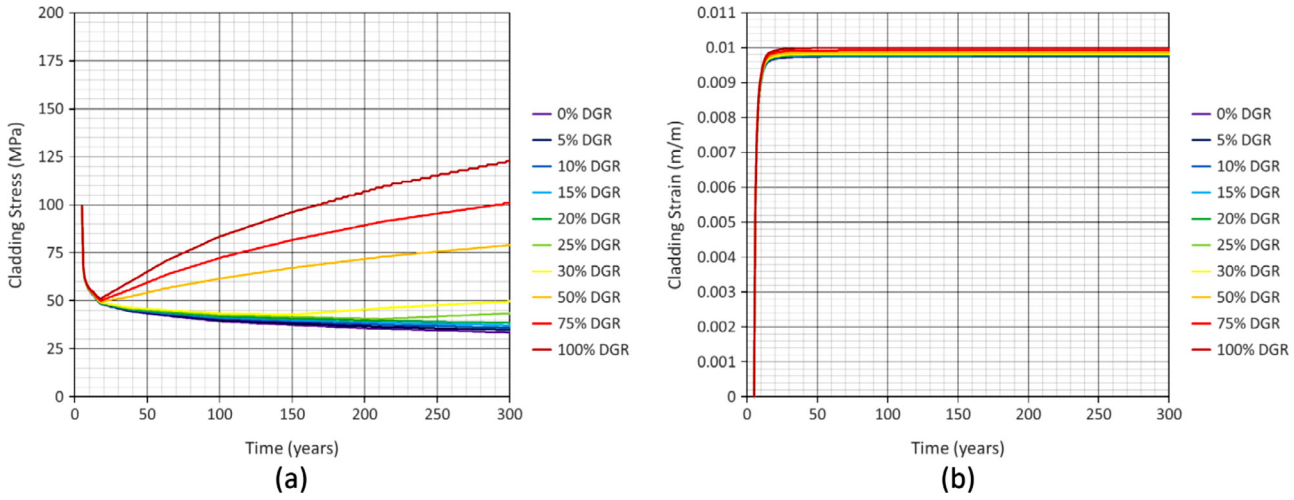

Fig. 7. Hoop stresses (left figure) and strains (right figure) in a PWR cladding calculated by Raynaud and Einziger with FRAPCON-DATING. Different colors correspond to different fractions of Decay Gas Release (DGR) assumed in the simulations. Figure from Raynaud and Einziger [28].

3.2.2. KAERI Analysis

A study on Korean spent fuel performed by Kim et al. [43] has revealed that the hoop stress at 400 °C of low burnup fuel (<45 GWd/tU) irradiated in Korean power plants remains below the 90 MPa limit proposed by NRC. However, the authors demonstrated that the hoop stress can reach 120 MPa in fuel assemblies exceeding 55 GWd/tU if the heat generation rate in the last cycle is high and therefore a high FGR occurred.

In the follow-up study, Kim et al. [44] have numerically studied RIP and hoop stresses at the beginning of dry storage with a conservative approach. Two types of fuel rods used in Korea have been investigated: 16x16 Combustion Engineering (CE) and 17x17 Westinghouse (WH). The authors used the fuel code FRAPCON-4.0 [45]. The simulations account for the base irradiation, wet storage and vacuum drying. For conservatism, the heat generation rate during the last cycle is the highest. However, RIP obtained with this approach exceeds the system pressure at burnups higher than 50 GWd/tU, and thus the power history for these cases have been adjusted to avoid this issue. The temperature of 25 °C is kept constant during the 5–year long wet storage period. Wet storage is followed by the vacuum drying up to 400 °C. The temperature during this procedure is assumed to be axially uniform. It must be emphasized that this assumption is not realistic. As mentioned in Section 2.1, the temperature axial distribution inside a cask is non-uniform. The authors used this assumption for the sake of conservatism. The simulations have been performed for the assembly average burnup range of 30-–60 GWd/tU.

The results obtained by the authors are presented in Fig. 8. The two figures show RIP and the average hoop stress at different burnups at 400 °C. As can be seen, the hoop stress in the WH rod exceeds the 90 MPa limit for burnups higher than 50 GWd/tU. In the case of the CE rod, the limit is crossed above 55 GWd/tU. The presented results have shown the importance of RIP on the cladding stress.

3.2.3. Cladding stresses in IFBA rods

Helium produced during irradiation of IFBA fuel is released to the rod free volume and contributes to RIP [32]. This is of importance in dry storage since high RIP can drive rod degradation mechanisms like reorientation of hydrides. The issue of RIP in IFBA rods during vacuum drying has been studied by Bratton et al. [46]. The authors used FRAPCON-3.5 [40] to simulate nearly 70,000 fuel rods from the Watts Bar nuclear plant. Bratton et al. simulated both IFBA and standard rods taking into account their unique irradiation histories. The obtained results have shown a significant impact of the helium production in IFBA fuel on RIP and, in consequence, the cladding hoop stress. The values of these parameters, calculated at vacuum drying conditions, are presented in Fig. 9. As can be seen, the RIPs and cladding hoop stresses is the IFBA rods can be around twice higher than in standard rods. The work of Bratton et al. clearly shows how important it is to account for each parameter potentially affecting the cladding stress distribution.

3.3. Fuel-cladding bonding

The fuel–cladding bonding is a phenomenon associated with high burnup fuels (> 45 GWd/tU). It occurs when the fuel outer surface interacts with the cladding inner surface. The mechanical contact leads to formation of the oxide layers of U, Zr and some fission products like Cs [47]. The layers create a strong mechanical bond between the pellet and the cladding. If the bond exists, the distribution of stresses in the cladding during storage and transportation conditions depends directly on the mechanical interactions between the fuel pellet and the cladding and not on RIP.

Recently, EPRI used the fuel codes BISON [48] and Falcon [49] to perform detailed numerical analyses of the impact of bonding on the cladding stresses during storage of PWR rods [50]. The simulations done by EPRI cover a wide range of high burnup fuel conditions by modeling various scenarios and using different crack patterns. An example of the cladding hoop stress calculated by EPRI with BISON is shown in Fig. 10. In the presented case, the simulated fuel rod is irradiated up to 60 GWd/tU and the bonding occurs. The base irradiation is followed by wet storage at 40 °C and vacuum drying up to 400 °C. The maximum temperature is kept for one year to observe the effect of the relaxation of stresses. Fig. 10 illustrates the distribution of the cladding hoop stress at the end of drying and after one year at 400 °C. It can be seen that the maximum hoop stress after relaxation is 12 MPa which is much below the hydrogen reorientation threshold at this temperature.

The overall results presented in the EPRI's report [50] have revealed that the presence of bonding significantly changes cladding stress distribution in storage conditions. Although, the cladding stresses in bonded rods reach high values, they are short-lived because of the cladding creep and the pellet constraint imposed on the cladding. The cladding at 400 °C has a high creep rate but its deformation is limited by the non-deforming fuel pellet. In response to this constraint, the cladding relaxes its stresses. The creep effect is beneficial in this time frame in this case. EPRI

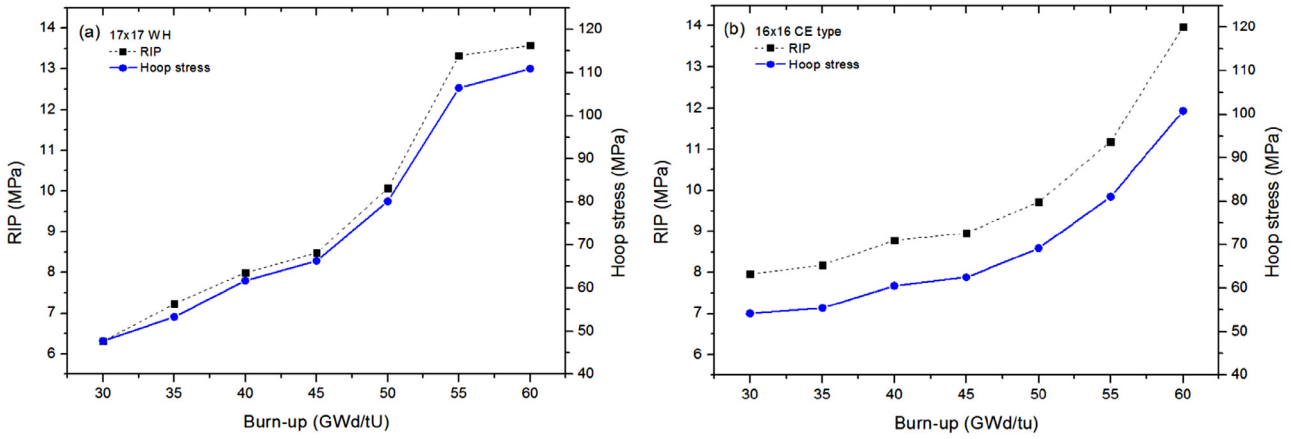

Fig. 8. RIP (left axis) and hoop stress (right axis) at 400 °C as a function of burnup calculated by Kim et al. for CE (right figure) and WH (left figure) fuel rods. Figure from Kim et al. [44].

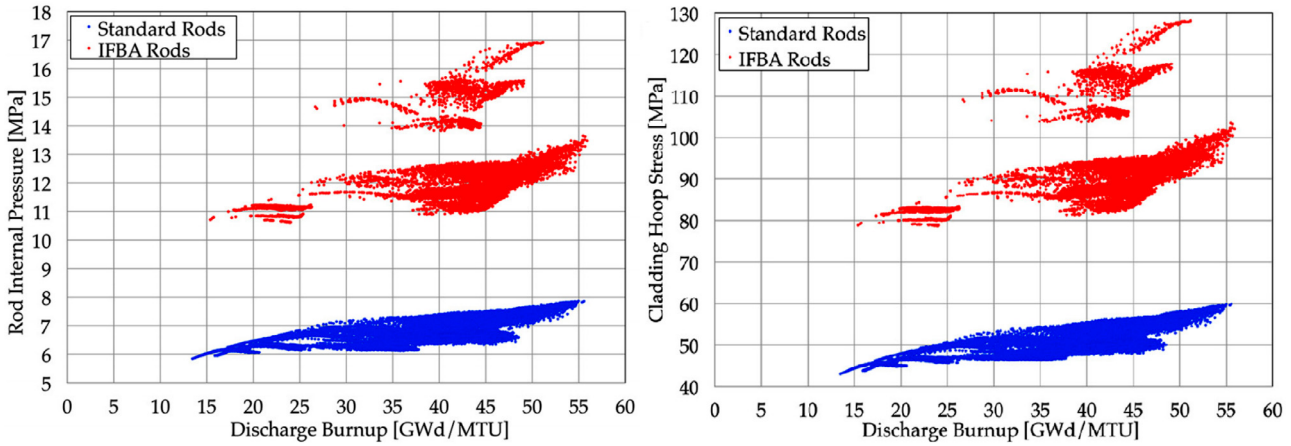

Fig. 9. Densities of RIPs (left figure) and hoop stresses (right figure) calculated at vacuum drying conditions (temperature 400 °C, external pressure 133 Pa) as a function of burnup. Red dots – standard rods, blue rods – IFBA rods. Figure from Bratton et al. [46]. (For interpretation of the references to colour in this figure legend, the reader is referred to the web version of this article.)

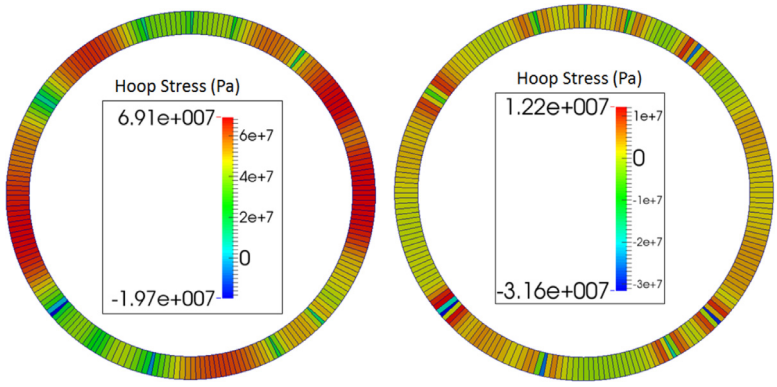

Fig. 10. Cladding hoop stress at 400 °C at the end of drying (left figure) and after one year of holding at 400 °C. Figure from [50].

has concluded that the high burnup fuel rods where the fuel and cladding are bonded appear to be more tolerant to hydride reorientation than non-bonded rods with lower burnup.

3.4. Long-term creep behavior

According to the spent fuel integrity research performed in the USA in the1970/s and1980/s, the cladding creep was identified as the most important limiting phenomenon in dry storage [51]. However, a more recent NRC report removes creep from the list of the most limiting phenomena [13]. It points out that the cladding creep in normal storage conditions will not lead to gross rupture of the cladding for two reasons. First, according to the post-storage tests carried out by Einziger et al, SNF exhibits a high creep capacity even after 15 years of dry storage [52]. Second, creep is self-limiting: progressing creep increases the rod volume which decreases RIP, which is the main force driving the cladding creep; as the driving force is lower, the creep rate decreases.

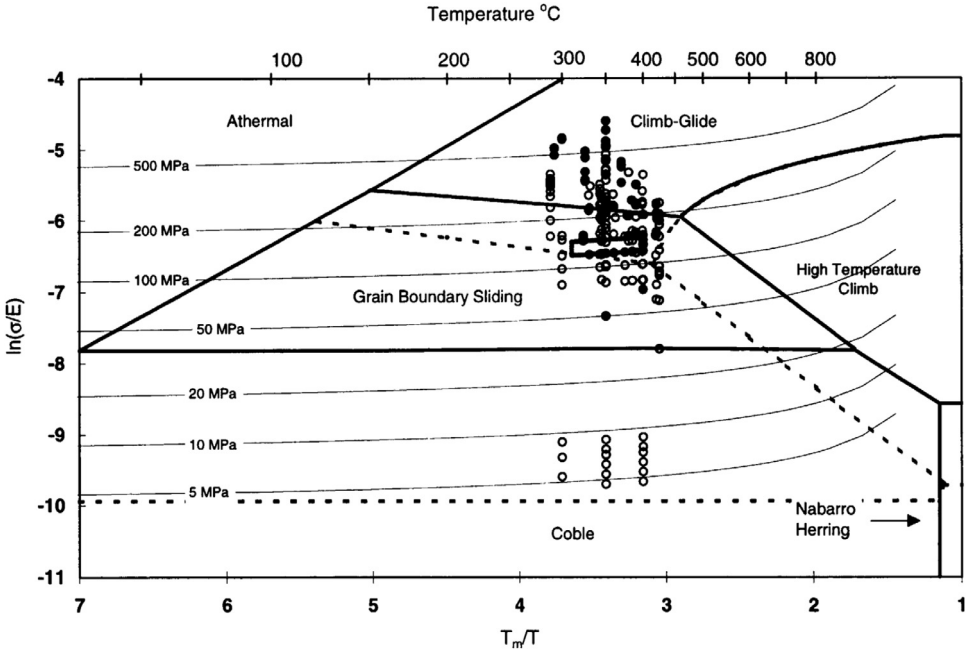

Fig. 11. Updated map of creep effects considered in DATING. The dashed lines give the temperature-stress boundaries for the model describing creep of fresh cladding. The solid rectangle shows the boundaries of the creep model of irradiated cladding. Experimental data used in the study are marked as points. Figure from Gilbert et al. [56].

Even though creep does not threaten the cladding integrity directly, it affects distribution of stresses [15,28]. The cladding stress is important in predicting the orientation of hydrides in dry storage [53,54]. Thus, it may be important to properly assess the cladding mechanical response in dry storage conditions.

3.4.1. Creep models from DATING

Since the cladding creep was believed in the1980ʃs to be the main failure mechanism during dry storage in the US, the Pacific Northwest National Laboratory developed a dedicated tool to predict the allowable temperature during dry storage DATING [41]. The code is a numerical implementation of the deformation and fracture map methodology proposed by Chin et al. [55]. DATING takes into account 6 creep mechanisms: High Temperature Climb (HTC), Low Temperature Climb (LTC), Grain Boundary Sliding (GBS), Nabarro-Herring creep, Coble creep and athermal creep. In the conditions typical for dry storage, HTC, LTC and GBS are the most important.

In the updated version of DATING, released by Gilbert et al. in 2001 [56], the model for primary creep has been included. Also, the coefficients of GBS, LTC and Coble creep models have been changed for unirradiated cladding. Finally, the creep reduction factor due to irradiation has been added to some creep mechanisms. The map of creep mechanisms considered in the updated version of DATING is shown in Fig. 11.

The updated creep models available in DATING have been recently applied by NRC to study fuel performance in dry storage conditions (see Section 3.2.1).

3.4.2. Czech creep model for Zircaloy-4 and Zr1Nb

One of the first attempts to model the long-term creep behavior under dry storage conditions based on dedicated experiments is the work of Vesely et al. [57]. The authors studied cladding samples of unirradiated Zr1Nb and Zry-4. The specimens used in the experiment were pressurized with pure argon and closed with welded caps. The samples prepared this way were divided into two groups that were heated up in a muffle furnace to different temperatures and in different environments. Also, the range of hoop stresses were different. The duration of the experiments was varying from 23 to 9600 hours, depending on the temperature.

The obtained experimental results have been used to describe the creep behavior with the overall hoop creep strain ε, consisting of two parts: the saturated transient strain ε_t^s and the steady state creep rate $\dot{\varepsilon}_s$.

$$\varepsilon = \varepsilon_t^s\left[1 - \exp\left\{-D(\dot{\varepsilon}_s t)^n\right\}\right] + \dot{\varepsilon}_s t \tag{11}$$

$$\dot{\varepsilon}_s = \frac{BE}{T}\exp\left(\frac{C\sigma}{E}\right)\exp\left(\frac{-Q}{RT}\right) \tag{12}$$

$$\varepsilon_t^s = \exp\left(FT + G\right)\dot{\varepsilon}_s^{HT+I} \tag{13}$$

$$D = K\exp\left(LT\right) \tag{14}$$

with

σ – applied hoop stress [MPa]

E – Young's modulus of Zr1Nb alloy ($E = 1.121 \times 10^5 - 64.4T$) [MPa]

T – Temperature [K]

Q – apparent activation energy [J/mol]

R – gas constant [J/mol]

The parameters B, C, F, G, H, I, K, L and n have been adjusted by the authors to fit the experimental measurements for normal (up to 400 °C) and abnormal conditions (above 420 °C). They are presented in Table 1.

The results of the fitting done by Vesely et al. for abnormal conditions is shown in Fig. 12. As can be seen, the hoop strains measured at 453 °C are well predicted with the model.

The work of Vesely et al. has been applied by Gyori and Hozer to model dry storage of VVER 440 fuel [58]. The authors implemented the model to the fuel code TRANSURANUS and performed multiphysics simulations. Their work is described in detail in Section 5.2.3.

3.4.3. EDF Creep model

A joint program aimed at studying the long term storage of nuclear fuel in France was launched by Commissariat á l'Energie

Table 1
Parameters of the Vesely creep model [57]. The first two rows give the temperature and hoop stress validity ranges.

Temperature	325 – 400 °C	420 – 530 °C
Hoop stress	50 – 110 MPa	40 – 130 MPa
B	130	8.718×10^6
C	2400	3900
D	$K = 56140$ $L = -9.547 \times 10^{-3}$	45
F	-7.82×10^{-2}	-7×10^{-2}
G	59.812	53.230
H	-2.4×10^{-3}	-2.77×10^{-3}
I	2.272	2.465
n	0.5	0.6
Q	1.85×10^5 J/mol	2.56×10^5 J/mol

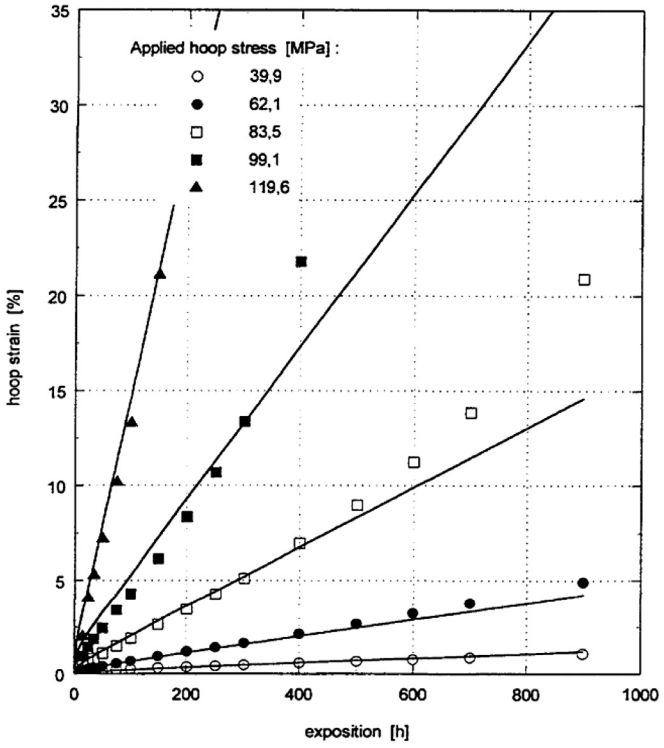

Fig. 12. The hoop strain calculated by Vesely et al. compared to the experimental measurements at 453 °C. Figure from Vesely et al. [57].

Atomique et aux énergies alternatives (CEA) and Électricité de France (EDF) in 1998 as the PRECCI project [2]. One of the activities done in the framework of PRECCI was formulation of a new cladding creep law to assess the cladding integrity under dry storage conditions. This model has been developed by Bouffioux for both fresh and irradiated CWSR (Cold Worked Stress Relieved) Zircaloy-4 claddings [59]. It is based on a set of experiments on pressurized cladding samples. The experimental procedure is similar to the one used by Vesely et al. [57].

A generic strain equation, expressed as a function of the hoop stress σ_θ [MPa], temperature T [°C] and time t [hours], used to fit the experimental data on unirradiated and irradiated cladding materials is as follows:

$$\varepsilon_\theta = \varepsilon_0(\sigma_\theta, T) f_{\varepsilon 0}(\phi t) \ln(1 + \nu t) + K(\sigma_\theta, T) f_K(\phi t) t \tag{15}$$

The first and second parts of the right side of Eq. 15 represent the primary and secondary creep components respectively. The parameters ε_0 and K are expressed as:

$$\varepsilon_0 = A_1 \sigma_\theta^{n1} \exp\left(\frac{-Q_1}{T + 273}\right) \tag{16}$$

Table 2
Range of validity of the EDF creep model [59].

Parameter	Value
Hoop stress (MPa)	55–230
Temperature (°C)	350–420
Fast fluence (n/cm^2)	(0–9)$\times 10^{21}$
Duration	100 h–approx. 2 y

Table 3
Parameters of the EDF creep model [59].

Parameter	Value
ν	0.13244
A_1	20867.2
n_1	1.986
Q_1	13748
A_2	1.386×10^{14}
n_2	1.715
Q_2	27628.7
a_0	0.01453
P_1	0.0879
P_2	0.9121
α_p	5.722×10^{-22}
S_1	0.00305
S_2	0.99695
β_s	3.246×10^{-22}

$$K = A_2 \exp\left(\frac{-Q_2}{T + 273}\right) (\sinh(a_0 \sigma_\theta))^{n2} \tag{17}$$

Irradiated cladding materials can be modeled with Eq. 15 by using the multiplying functions $f_{\varepsilon 0}(\phi t)$ and $f_K(\phi t)$ that take into account the effect of fast fluence ϕt [n/cm^2]:

$$f_{\varepsilon_0}(\phi t) = P_1 + P_2 \exp(-\alpha_p \phi t), \quad P_1 + P_2 = 1 \tag{18}$$

$$f_K(\phi t) = S_1 + S_2 \exp(-\beta_s \phi t), \quad S_1 + S_2 = 1 \tag{19}$$

Eq. 15 is valid for both fresh and irradiated cladding in the range of values given in Table 2.

The empirical coefficients used in Eq. 15–19 have been adjusted to fit the experimental data. Their values are listed in Table 3. The EDF creep model gives a good prediction of hoop strains in fresh and irradiated CWSR Zircaloy-4. The comparison for irradiated samples is presented in Fig. 13. The strain evolution of samples irradiated to different levels is well captured by the model. The solid blue curve representing the fresh cladding material is added for comparison. It shows that the ductility decrease caused by irradiation is properly modeled with the EDF creep law.

3.4.4. CIEMAT Creep model

The EDF creep model proposed by Bouffioux reproduces the experimental measurements with a great precision but is relatively complex. The data used to fit the EDF model have been used by Herranz and Feria from CIEMAT (Centro de Investigaciones Energéticas, Medioambientales y Tecnológicas) to propose a new, simplified creep model [60]. The authors have chosen the mathematical form of the model that is consistent with the default creep formulation available in the fuel code FRAPCON [61] to facilitate further implementation.

$$\dot{\varepsilon}_\theta = f_1(\sigma_\theta) f_2(T) f_3(\phi t) t^{-0.5} \tag{20}$$

The CIEMAT creep law described with Eq. 20 consists of three functions f_1, f_2 and f_3 that give dependencies on the hoop stress σ_θ [MPa], temperature T [°C] and fast fluence ϕt [n/cm^2]:

$$f_1(\sigma_\theta) = 1/2 a \sigma_\theta^b \tag{21}$$

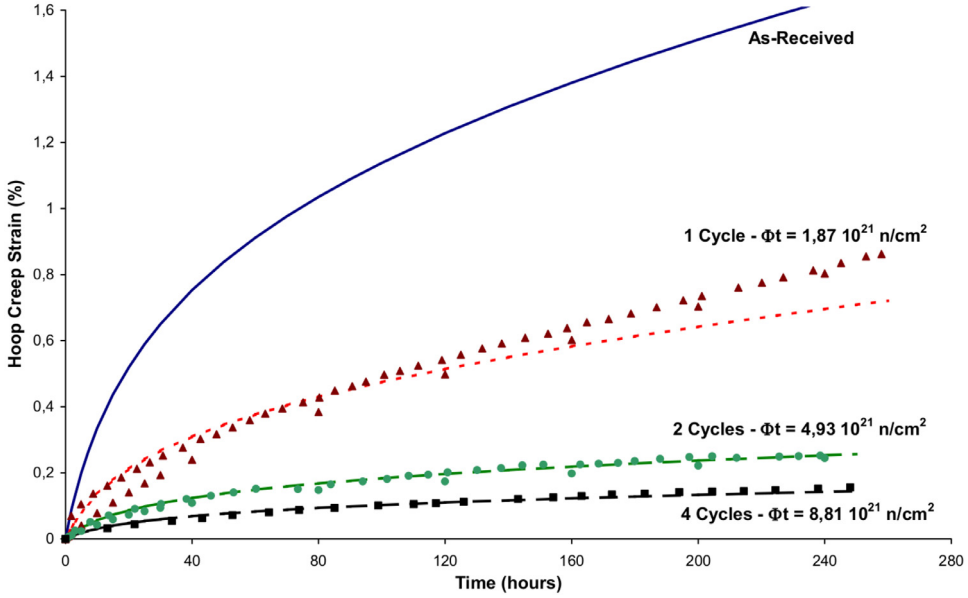

Fig. 13. Hoop strains calculated with the EDF creep law (lines) compared to experimental data on irradiated CWSR Zircaloy-4 samples (points). The solid blue curve shows the hoop strain evolution of fresh cladding. Figure adapted from Bouffioux [59]. (For interpretation of the references to colour in this figure legend, the reader is referred to the web version of this article.)

Table 4
Parameters of the CIEMAT creep model [60].

Parameter	As-received	Irradiated
a	6×10^4	300
b	1.84	2.95
c	15000	15000
d	0	2.8×10^{-22}

$$f_2(T) = \exp\left(\frac{-c}{T+273}\right) \tag{22}$$

$$f_3(\phi t) = \exp\left(-d\phi t\right) \tag{23}$$

The coefficients a, b, c and d are used to fit Eq. 20 to the experimental data used by Bouffioux [59]. The fitted values obtained by Herranz and Feria are shown in Table 4.

The comparison of the EDF and CIEMAT creep models with the experimental measurements is presented in Fig. 14. As can be seen, the experiments on both fresh and irradiated cladding samples are well predicted by the CIEMAT model. Herranz and Feria have succeeded to combine a sufficient precision with simplicity. 14 coefficients used in the EDF model have been reduced to 4 coefficients in the CIEMAT model which eases integration into fuel performance codes.

3.5. Hydrogen behavior

Fuel rods undergo slow waterside corrosion during reactor operation. It is associated with hydrogen absorption by the cladding material [19]. Once absorbed, hydrogen diffuses and changes its chemical state depending on the local conditions. It can occur in solid solution or precipitate into hydrides. Hydrogen in solid solution undergoes redistribution driven by temperature, concentration and stress gradients. If precipitated, hydrogen can significantly affect mechanical properties of the cladding and can activate degradation mechanisms like embrittlement and DHC.

3.5.1. Hydrogen precipitation and dissolution

Hydrogen absorbed by the cladding can occur under different forms. It can be either dissolved in the solid solution or precipitate as radial or tangential hydrides. Hydrogen is dissolved in the solid solution phase if its concentration is below the Terminal Solid Solubility for dissolution (TSSd) C_{TSSd} and it precipitates as hydrides if its concentration is higher than the Terminal Solid Solubility for precipitation (TSSp) C_{TSSp}. TSSd and TSSp curves are presented schematically in Fig. 15.

One can see that these curves are different in thermal cycling. Such behavior is called hysteresis. Hysteresis of the hydrogen solubility can be explained by the different quantity of energy consumed in the dissolution and precipitation processes. Hysteresis is discussed in more detail in [63] and [64]. C_{TSSd} and C_{TSSp} can be expressed with the following equations:

$$C_{TSSd} = A\exp\left(\frac{-Q}{RT}\right)\ [\text{wppm}] \tag{24}$$

$$C_{TSSp} = A\exp\left(\frac{-Q}{RT}\right)\ [\text{wppm}] \tag{25}$$

where R [J mol^{-1} K^{-1}] is the gas constant and T [K] is temperature. The coefficients A and Q can be determined from thermal cycling experiments. Examples of these coefficients proposed by different authors are listed in Table 5.

Parameters presented in Table 5 vary because they are based on different sets of experimental data and they were fitted by different authors according to their needs. The C_{TSSd}/C_{TSSp} curves listed in Table 5 are plotted together in Fig. 16 for comparison.

To model dissolution and precipitation of hydrogen, one needs to take into account kinetics of these two phenomena. Whereas the dissolution process is very rapid and most authors assume that equilibrium is maintained, the kinetics of precipitation cannot be neglected. According to Marino [70], the hydrogen precipitation can be expressed with the following equation:

$$\frac{dC_{ss}}{dt} = -\alpha^2\left(C_{ss} - C_{TSSp}\right) \tag{26}$$

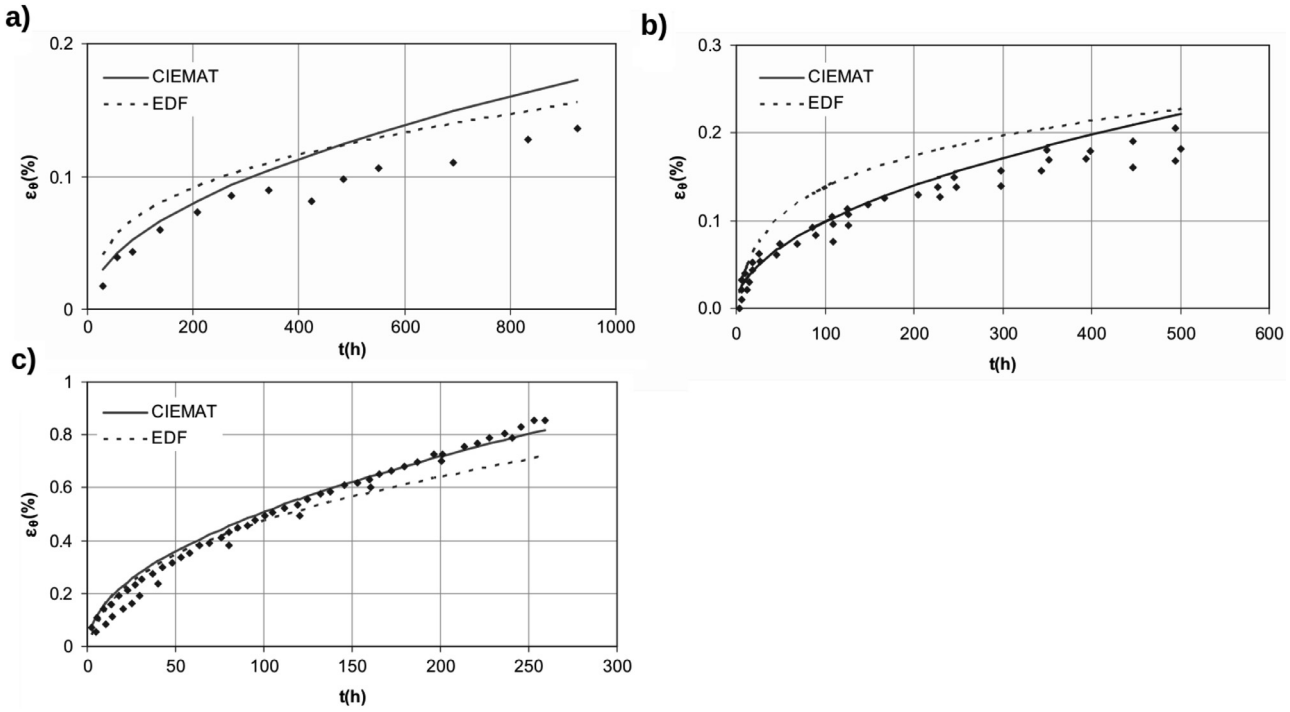

Fig. 14. Hoop strains calculated with the EDF (dashed lines) and CIEMAT (solid lines) creep models compared to experimental data from [59]. Fast fluence, stress and temperature of studied samples in subplots: a) 8.8 × 10^{21} n/cm^2, 140 MPa, 380 °C, b) 0 n/cm^2, 100 MPa, 350 °C, c) 1.9 × 10^{21} n/cm^2, 121 MPa, 400 °C. Figures from Herranz et al. [60].

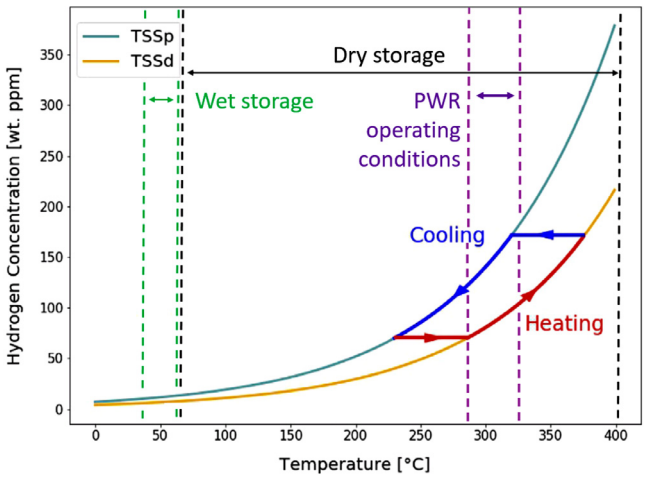

Fig. 15. Hydrogen dissolution/precipitation scheme. The red and blue arrows indicate the process direction. Ranges of temperatures typical for wet storage, dry storage and PWR operating conditions are marked by vertical, dashed lines. Figure adapted from Kaufholz et al. [62]. (For interpretation of the references to colour in this figure legend, the reader is referred to the web version of this article.)

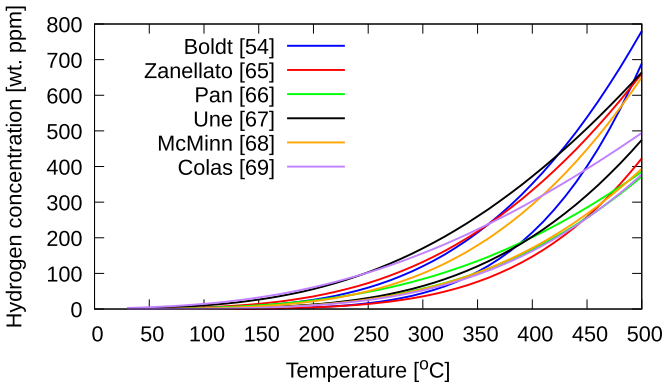

Fig. 16. Hydrogen precipitation (dashed lines) and dissolution (solid lines) plotted with data from Table 5.

where C_{ss} is the concentration of hydrogen in solid solution and α is the kinetics parameter which has the Arrhenius form:

$$\alpha = A_\alpha \exp\left(\frac{-Q_\alpha}{RT}\right) \tag{27}$$

Most authors working on hydrogen behavior use the values of A_α and Q_α proposed by Kammenzind et al. [71]. However, it is worth to mention the precipitation kinetics derived by Boldt et al. [54], Une and Ishimoto [72] and Zanellato et al. [65].

A recent work of Lacroix et al. presents a new approach to the modeling of dissolution and precipitation of hydrides [73]. The Hydride Nucleation-Growth-Dissolution (HNGD) model derived by the authors has several new features. It distinguishes two precipitation mechanisms. The nucleation of hydrides is a rapid process occurring if the local hydrogen concentration in solid solution exceeds C_{TSSp}. The second mechanism, the growth of hydrides, is slower and can occur simultaneously with nucleation. Moreover, the growth occurs also in the hysteresis region. Next feature of HNGD is the introduction of the dissolution kinetics. Contrary to the previous model available in BISON [74], this process is not considered to be instantaneous. The model proposed by Lacroix et al. is schematically explained in Fig. 17. The HNGD model has been implemented into the fuel performance code BISON and tested by Passelaigue et al. [75].

3.5.2. Hydrogen diffusion

If the local hydrogen concentration in the cladding is below TSSd, hydrogen is dissolved in the lattice and takes interstitial positions. Hydrogen in solid solution can diffuse. The two main forces driving hydrogen redistribution are concentration (Fickian diffu-

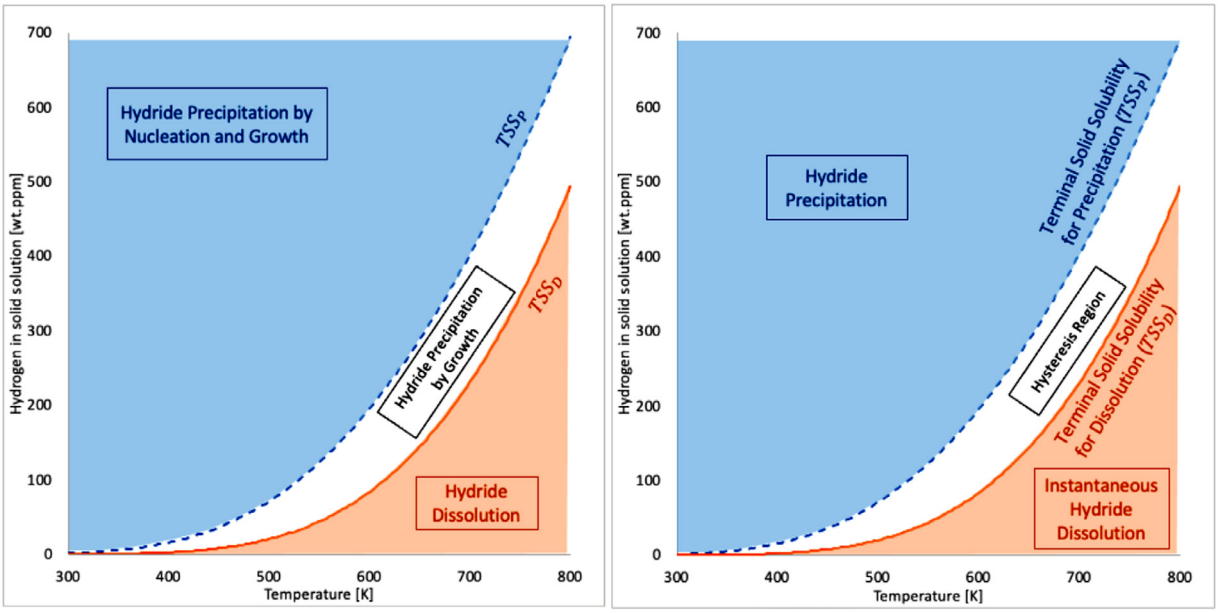

Fig. 17. Hydrogen concentration as a function of temperature. Left figure explains the assumptions of the HNGD model and the right one presents the previous modeling approach available in BISON [74]. Figure from Passelaigue et al. [75].

Table 5
Chosen hydrogen precipitation and dissolution parameters available in the literature. A and Q are parameters of Eqs. 24 and 25.

Parameter	A	Q	Material	Reference
C_{TSSd}	1750000	50383	Zircaloy-4	[54]
C_{TSSp}	166495	34467		
C_{TSSd}	510800	45610	Zircaloy-4	[65]
C_{TSSp}	66440	29630		
C_{TSSd}	80000	34520	Zr-2.5Nb	[66]
C_{TSSp}	30000	27990		
C_{TSSd}	143000	36686	Zircaloy-2	[67]
C_{TSSp}	32700	25042		
C_{TSSd}	106447	35991	Zircaloy-2,4	[68]
C_{TSSp}	138746	34469		
C_{TSSd}	108150	36360	Zircaloy-2	[69]
C_{TSSp}	13320	21170		

sion) and temperature (Soret effect) gradients. The stress-driven diffusion is neglected by most authors. A generic equation describing the diffusion of hydrogen J_H under these two gradients is given by:

$$J_H = -D\nabla C_{ss} - \frac{DC_{ss}Q^*}{RT^2}\nabla T \tag{28}$$

The first part on the right side of Eq. 28 corresponds to the Fickian diffusion and the second one to the Soret effect. D is the hydrogen diffusion coefficient, C_{ss} is the concentration of hydrogen in solid solution, Q^* is the heat of transport of hydrogen, R is the gas constant and T is temperature.

The diffusion coefficient D can be expressed with the Arrhenius equation:

$$D = A\exp\left(\frac{-B}{RT}\right)\ [\mathrm{m}^2\ \mathrm{s}^{-1}] \tag{29}$$

where A and B are the coefficients based on experimental data. The diffusion rate of hydrogen in different zirconium alloys has been studied by several authors. Some sets of the coefficients A and B are listed in Table 6 and plotted in Fig. 18 for comparison.

Different values of Q^* have been reported in the literature. They are gathered in Table 7.

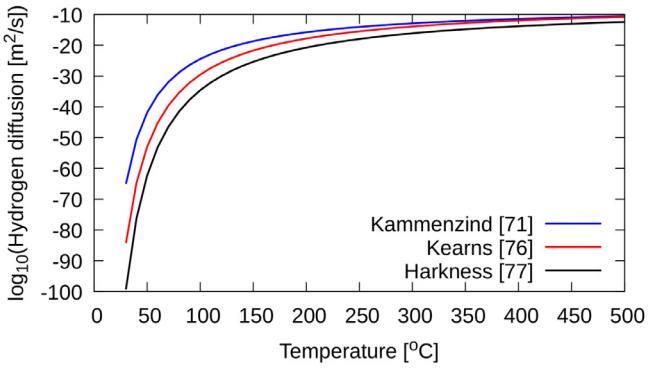

Fig. 18. Decimal logarithms of the hydrogen diffusion coefficients listed in Table 6 plotted as a function of temperature.

Table 6
Chosen hydrogen diffusion parameters available in the literature. A and B are parameters of Eq. 29.

Parameter	Value	Material	Phase	Reference
A	0.8×10^{-7}	Zircaloy-4	α	[71]
B	3.33×10^{4}			
A	7.90×10^{-7}	Zircaloy-2,4	α	[76]
B	4.49×10^{4}			
A	1.3×10^{-7}	Zirconium hydride	δ	[77]
B	5.31×10^{4}			

Table 7
Chosen hydrogen heat of transport values available in the literature.

Parameter	Value [kJ/mol]	Material	Phase	Reference
Q^*	25.1	Zircaloy-4	α	[71]
Q^*	25.1	Zircaloy-2	α	[78]
Q^*	30	Zircaloy-4	α	[79]
Q^*	5.43	Zirconium hydride	δ	[77]

An example of a hydrogen redistribution model has been proposed by Courty et al. [74]. The authors developed balance equations to model hydrogen diffusion, precipitation and dissolution. Their work has been implemented in the fuel performance code

BISON and applied to study multidimensional behavior of hydrogen during reactor operation and dry storage [80–82]. Recently, the Courty's model has been replaced by a new model proposed by Lacroix et al. [73] and implemented by Passelaigue et al. [75]. The main advantage of the Lacroix model is a new approach to the precipitation and dissolution of hydrides. The model has been validated by simulating experimental data and gave better results than the model proposed by Courty et al. Details of the model developed by Lacroix et al. are given in Section 3.5.1.

Besides diffusion in solid solution, one may also model hydrogen movement in hydrides. Veshchunov et al. have pointed out that, in the outer rim of high burnup fuels, cladding hydrides are precipitated in high quantities [83]. Their volume fraction f can exceed 50% and the movement of hydrogen within them is not negligible. The authors described the two phase hydrogen transport with the following equation:

$$J_H = J_{Zr}(1-f) + J_\delta f \tag{30}$$

where J_{Zr} and J_δ are fluxes of hydrogen in the zirconium lattice and in the precipitate, respectively. Both can be expressed with Eq. 28.

The hydrogen diffusion thorough a two-phase region has been also taken into account by Feria and Herranz [84]. In their work, the authors studied the impact of the oxidation front on the hydrogen migration. In this phenomenon, zirconium hydride is converted into oxide and the affected hydrogen undergoes dissolution, diffusion and re-precipitation. According to the experimental observations, hydrogen is pushed by the oxidation front towards inner parts of the cladding [85].

3.5.3. Hydride reorientation

When the local concentration of hydrogen exceeds the solubility limit, hydrogen precipitates into hydrides. Those can have different special orientations depending on the local conditions like temperature, stress or the material texture. During dry storage, one can expect tensile stresses in the cladding which favors radially oriented hydrides. Their high concentration can embrittle the cladding and lead to DHC. Several approaches to the hydride reorientation modeling can be found in the open literature. Some of them are briefly described in this section.

Chu et al. have proposed a hydride reorientation model based on their own experimental work [86]. Chu et al. thermo-cycled several Zircaloy-4 samples charged with different concentrations of hydrogen and derived a temperature- and stress-dependent model matching the obtained experimental data.

A very detailed hydrogen behavior model has been developed by Kolesnik et al. [87]. It accounts for many effects affecting reorientation of hydrides. First, the model distinguishes radial and circumferential hydrides already in the precipitation process. The authors assume that the stack of hydrides has two branches, one for each type of hydride. The orientation of precipitated hydrides depends on the hydride nucleus volume, applied stress and unconstrained misfit strains. The mentioned strains are associated with the formation of hydrides in α–Zr and their values are different for radial and circumferential hydrides. According to the model developed by Kolesnik et al., the different values of the unconstrained misfit strain with respect to crystallographic orientation also affect C_{TSSp} which is different for radial and circumferential hydrides. Another important phenomenon taken into account by Kolesnik et al. is the memory effect. The hydride formation process is associated with the emission of dislocation loops near the hydride. These loops stay in the matrix even if the hydride is dissolved. They can be partially annealed if exposed to high temperatures for a long time. New hydrides precipitating near the unannealed loops have tendency to occur with the same orientation as the previous ones. This phenomenon, called the memory effect, can be enhanced by the emission of loops and decreased by annealing caused by self-diffusion of zirconium atoms. As proven in the experimental work of Kulakov et al. [88], hydrides submitted to high stresses and temperatures during a long period of time can reorient without dissolution in the metal matrix. Kolesnik et al. have taken this phenomenon into account by modeling the flux of hydrogen from tangential to radial hydrides. Orientation of hydrides also depends on the alloy texture if no external stresses are applied. The model developed by Kolesnik at al. accounts for this phenomenon by introducing the so-called textural factor. The model proposed by Kolesnik et al. has been validated against several experimental works. An example of the thermal cycling experiment aimed at studying reorientation of hydrides [86] reproduced with the model is shown in Fig. 19. In the experiment, the Zircaloy-4 tubes were charged with different concentrations of hydrogen and pressurized to 160 MPa. A single thermal cycle accounted for a heating up to 400 °C, 2 h of holding time and cooling to 170 °C with the rate 1 °C/min. One can see that the fraction of radially oriented hydrides is sufficiently well predicted with the model, even if the samples underwent several thermal cycles.

Another hydride reorientation model has been proposed by Desquines et al. [89]. The authors based their model on the data obtained from compression tests carried out on unirradiated stress-relieved-annealed Zircaloy-4 samples charged with different hydrogen concentrations. The samples underwent mechanical and thermal treatment to provoke reorientation of hydrides. The obtained data has been used to determine the impact of temperature, stress and hydrogen concentration on the precipitation of radial hydrides. The model derived by Desquines et al. has been successfully implemented into the hydrogen behavior module of FRAPCON-3xt and validated by Feria et al. [53].

Hydride reorientation has been also taken into account in the hydrogen behavior model implemented into TESPA-ROD by Boldt [54]. The orientation criterion used by the author depends on the biaxial stress and temperature gradient in the cladding and it is based on the results obtained in the frame of an extensive experimental program at the Pennsylvania State University. The Penn State researchers studied hydrogen reorientation during cooling with the presence of a mechanical load which represents vacuum drying conditions [90,91]. According, to the obtained results, the primary stress (σ_1) threshold for reorientation decreases with the increasing secondary stress (σ_2), i.e. with the increasing the stress biaxiality ratio σ_2/σ_1 as shown in Fig. 20.

3.5.4. Delayed hydride cracking

Currently, DHC is considered one of the major degradation mechanisms during dry storage in both BWR and PWR fuel rods [92,93]. This slow-cracking phenomenon can lead to gross ruptures and occur even at low temperatures, which is of importance if the extension of dry storage is considered.

DHC begins when the stress intensity exceeds the threshold named the stress intensity factor K_{IH}. Publications concerning this parameter have been reviewed by Kim et al. [44]. The authors reported that the available experimental data for Zircaloy-2 and Zr-2.5Nb allow to assume a conservative value of $K_{IH} = 5$ MPa$\sqrt{m}$ [94]. Less experimental data for Zircaloy-4 has been published. According to the recent experimental results from the IAEA coordinated program, K_{IH} takes values of around 5–6 MPa$\sqrt{m}$ for temperatures between 250 and 295 °C [95,96]. Then, it increases significantly above 295 °C. Kim et al. has concluded that such values of K_{IH} lead to unrealistic crack sizes that would not occur in SNF.

Shi and Plus have derived a theoretical model predicting K_{IH} [97]. It is based on the assumption that the hydride fracture occurs only if the local stress threshold is reached. The values predicted by the model are in the vicinity of the experimental measurements obtained in the frame of the IAEA coordinated research

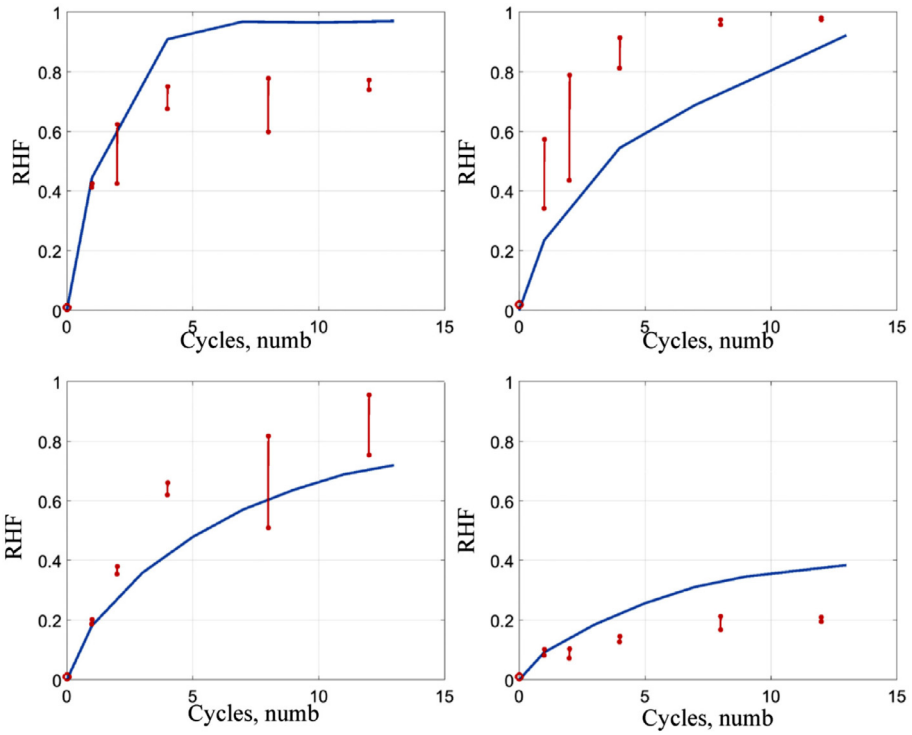

Fig. 19. Fraction of radial hydrides (RHF) as a function of the number of thermal cycles. Simulated values (lines) compared to the experimental results from Chu et al. [86]. Hydrogen content is different in subplots. Figure from Kolesnik et al. [87].

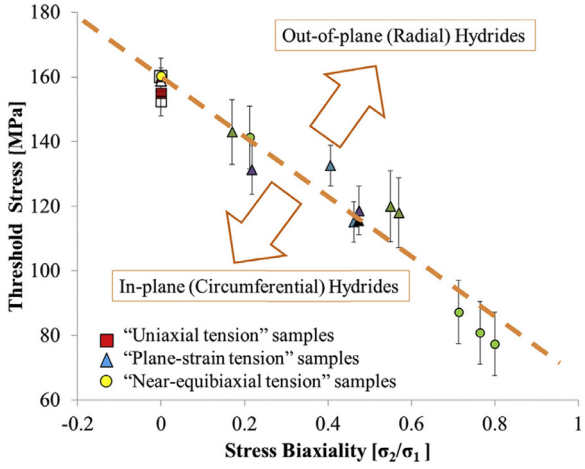

Fig. 20. Principal stress (σ_1) threshold for hydride reorientation during cooling of a sample charged with hydrogen as a function of stress biaxiality. Figure from Cinbiz et al. [91].

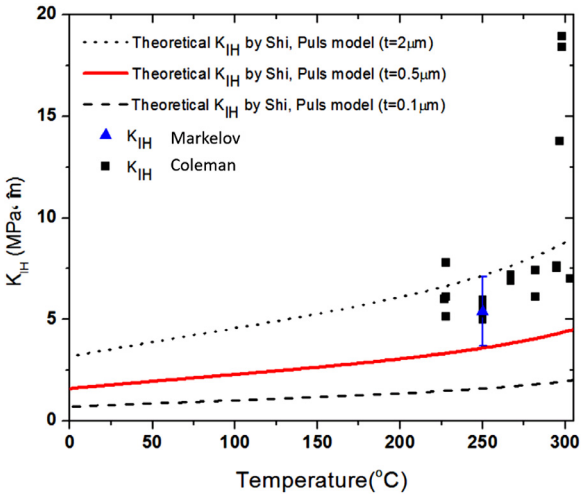

Fig. 21. Stress intensity factor measured by Markelov et al. [95] (in blue) and Coleman et al. [96] (in black) compared to the theoretical model derived by Shi and Plus [97]. t is the hydride thickness. Figure adapted from Kim et al. [44]. (For interpretation of the references to colour in this figure legend, the reader is referred to the web version of this article.)

program [95,96]. The comparison done by Kim et al. is shown in Fig. 21.

Raynaud and Einziger studied the critical flaw size a_{DHC}^{crit} instead of the stress intensity factor K_{IH} in their fuel performance simulations (see Section 3.2.1). These two parameters are related in the following way:

$$a_{DHC}^{crit} = \frac{1}{\pi} \times \left(\frac{K_{IH}}{\sigma Y\left(a_{DHC}^{crit}\right)} \right)^2 \tag{31}$$

where σ is the cladding hoop stress and $Y\left(a_{DHC}^{crit}\right)$ is the geometry factor. The authors used the above equation to calculate the critical flaw sizes for both BWR and PWR rods. The obtained results have shown that the values of a_{DHC}^{crit} are too large to cause a cladding failure during 300 years of dry storage [28].

This section is focused on approaches to predict DHC that can be easily applied to fuel performance modeling. However, numerous models have been developed to study DHC in zirconium-based materials at different scales. It is worth to mention the model based on the extended finite element method developed by Suman et al. [98,99] or the multi-physics modeling done by Xia et al. [100]

3.5.5. Other approaches to hydrogen behavior modeling

Besides fuel pellet-scale models described in previous sections, alternative ways are available. Techniques like Density Function Theory (DFT) or Molecular Dynamics (MD) can be employed to study hydrogen behavior at atomic scale and phase field modeling can be used to investigate micro-structure evolution of hydrides.

An example of atomic scale calculations is the work of Zhang et al. [101] who used Kinetic Monte Carlo (KMC) simulations to predict the hydrogen diffusion measured by Ishioka and Koiwa [102] with a great precision. KMC has also been used by Liyange et al. to study the impact of oxygen on hydrogen diffusion [103]. The authors concluded that the presence of interstitial oxygen atoms in the zirconium lattice decreases the hydrogen diffusivity.

As an example of phase field modeling applied to hydrogen behavior studies it is worth to mention the works done by Shi and Xiao [104] and Xiao et al. [105] on hydrogen precipitation. The authors have studied the evolution of δ and γ hydrides in zirconium in real time and real length scale. They identified crucial parameters governing hydride morphology like hydride nucleation rate or hydride supersaturation.

It must be emphasized that it would be is difficult to directly employ the techniques mentioned above to fuel performance analysis because the computational cost is currently too high. However, atomic scale and phase field modeling can provide crucial insights on these aspects of hydrogen behavior that have not been fully understood yet. For instance, the orientation of hydrides, important in predicting the crack propagation in the cladding at macro-scale, is a multi-scale problem requiring atomic scale analysis, phase field modeling and experimental observations. More examples of the micro- and meso-scale modeling of hydrogen behavior have been given by Motta et al. [19].

3.6. Transportation issues

SNF is transported at least once within its life cycle, either from an on-site storage pool to an interim storage facility or directly to a final repository. Transportation is associated with vibrations leading to fatigue which may affect rod integrity in the subsequent storage/disposal. As shown by Wang et al. [106] (see Section 4.4), the mechanical behavior and time to fatigue failure of SNF submitted to cyclic vibrations strongly depend on many factors such as burnup, oxide thickness, bonding efficiency and stress history. High fidelity estimations of such parameters can be obtained with fuel performance codes. These can be helpful in designing experiments or generating realistic boundary conditions for mechanical simulations of transportation or drop accidents, not qualifying as fuel performance modeling. On the other hand, such mechanical simulations as well as the experimental observations can be used to derive mechanical fatigue correlations to be implemented in fuel performance codes or gain insights on other phenomena. For instance, the mechanical modeling of the bonding effect done by Almomani et al. [107,108] or by Jiang et al. [109] and the experimental data [106] can be used to derive new bonding models or improve existing ones.

4. Experiments supporting dry storage modeling

Ongoing and planned experiment that could help to understand processes occurring during dry storage are shortly discussed in this section.

4.1. Long-term creep

Currently, a project aimed at developing physical models for safety justification of spent nuclear fuel dry storage is ongoing in Russia [4]. In the frame of the project, dimensional changes of spent fuel rods during dry storage are studied [110]. Aliev et al. have developed a new creep model and validated it against available data. However, the used experimental results, marked by empty rectangles in Fig. 22, do not cover the range of values normally expected in dry storage. In order to provide missing data covering the desired range of conditions, marked by the gray area, a research program has been launched at the Kurchatov Institute, SSC TRINITI and SNC RF RIAR.

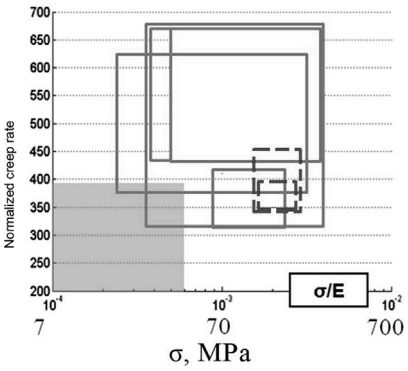

Fig. 22. Map of experimental data used for model verification. The filled area corresponds to dry storage conditions. The empty rectangles with solid borders correspond to fresh cladding and dash borders to irradiated cladding. Vertical axis–normalized creep rate, horizontal axes–hoop stress σ and the hoop stress to Young's modulus ratio σ/E. Figure from Aliev et al. [110].

4.2. Hydrogen behavior

The Swiss nuclear landscape includes several types of fuel rods. Currently, both PWRs and BWRs are operated in Switzerland generating power from both MOX and standard UO_2 fuel pellets. Moreover, different types of cladding materials are used. Besides the widely used and studied Zircaloy-4, the Swiss nuclear industry uses duplex claddings. Zircaloy-2 with an inner layer (LK3/L) is used in BWRs and Zircaloy-4 with an outer layer (DXD4) in PWRs. The presence of liners has an impact on the hydrogen behavior and mechanical performance. Such a variety of fuel/cladding combinations requires extensive experimental work to support future dry storage. Most of the experiments are done at Laboratory for Nuclear Materials of Paul Scherrer Institute (PSI) in Switzerland. Conducted experimental research concerns the hydrogen behavior and mechanical properties of zirconium alloys.

4.2.1. Zircaloy-2 with inner liner

Duarte et al. studied the behavior of hydrogen in the Zircaloy-2 samples with and without the inner liner [6]. The authors carried out C-shaped ring compression tests on the cladding samples charged with hydrogen. The light optical microscopy examination of the Zircaloy-2 without a liner revealed that hydrides precipitate uniformly and most of them are circumferential. In the sample with a liner, the distribution of hydrides is different. Hydrogen tends to accumulate near the liner–substrate. Also, the circumferential hydrides are not distributed uniformly. Lower concentration of them occurs near the middle part of the sample. Radially oriented hydrides are formed near the cladding outer surface.

The light optical microscopy of both samples is shown in Fig. 23. The load-displacement curves recorded by the testing machine during the compression tests are used to study the difference in the mechanical performance of the specimens. The obtained results have shown that the inner liner has little impact on the mechanical behavior.

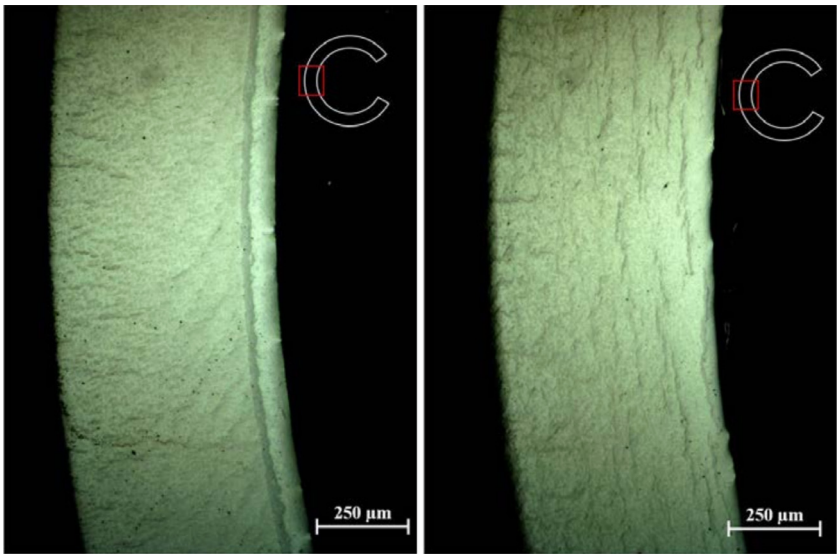

Fig. 23. Light optical microscopy images of the sample without liner (right figure) and with liner (left figure). Figure from Duarte et al. [6].

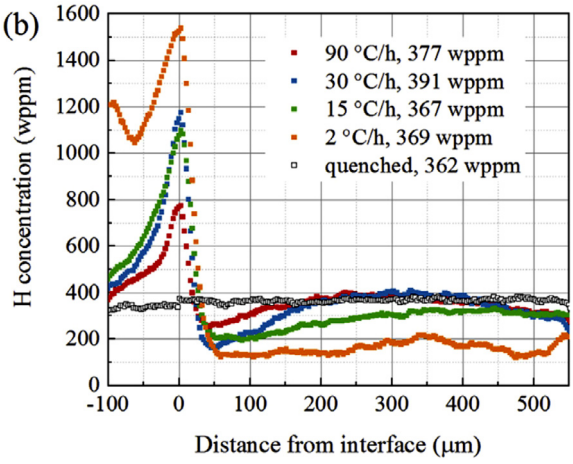

Fig. 24. 1D quantification of the hydrogen concentration radial profiles. Initial hydrogen content 350 wppm. Figure from Gong et al. [111].

4.2.2. Zircaloy-4 with outer liner

The DX-D4 cladding has also been studied at PSI. This type of cladding consists of a low-tin Zircaloy-4 outer liner bonded to a standard Zircaloy-4 inner substrate. Gong et al. investigated hydrogen diffusion and precipitation in DX-D4 samples cooled from 400 °C to 100 °C with different cooling rates [111]. In the experiment, two cladding tubes were charged with hydrogen up to 200 and 350 wppm. In the next step, both tubes spent 34 hours at 500 °C to ensure homogeneous distribution of hydrogen. Then, each tube was cut into several specimens. All of them were heated up to 400 °C and spent 10 h at this temperature, which was followed by temperature transients. The samples were cooled down with different cooling rates and quenched. After the heat treatment, the specimens were analyzed with the PSI Neutron Microscope [112,113]. The neutron radiographs of the samples charged with 350 wppm of hydrogen and cooled down with different rates have shown that the absorbed hydrogen tends to gather near the liner inner wall. This effect is stronger for lower cooling rates. The hydrogen content quantification in the studied samples has been done by the authors. Fig. 24 presents 1D hydrogen concentration profiles of the samples with 350 wppm of hydrogen. According to the obtained results, the highest concentration of hydrogen is at the interface and it decreases towards both side. However, the hydrogen profiles in the liner show concentration gradients whereas the distribution in Zircaloy-4 is uniform.

The two experiments briefly described in this section have proven that the hydrogen behavior in duplex claddings significantly differs from standard ones, and thus it will require separate models to be properly anticipated.

4.3. Slow cooling rate effect

In general, the cooling rate of SNF in dry storage is extremely low. An example given in [114] shows that the cooling rate of the fuel rod irradiated to 45 GWd/tU is around 3 °C/year during first 100 years. Such a cooling rate is considerably lower than a typical cooling rate in laboratory experiments.

The effect of the low cooling rate on the cladding performance is currently being experimentally studied by KAERI [115]. In the experimental procedure, the cladding specimens are charged with different concentrations of hydrogen and pressurized to reach different hoop stresses. Then, the specimens are divided into three groups and submitted to the cooling process lasting 3, 6 and 12 months with the initial temperature of 400 °C. These three groups have the cooling rates 0.109, 0.054 and 0.027 °C/hour respectively. The experimental setup is presented in Fig. 25. At the moment, the full set of experimental results have not been published. However, the preliminary results indicate that the samples with a lower cooling rate exhibit more ductile behavior than the samples cooled faster.

4.4. Fatigue during transportation

The cladding/rod integrity during transportation in dedicated casks can be affected by vibrations and impact loading resulting in mechanical fatigue. The rod performance depends on many factors like the oxide layer thickness, hydrogen concentration, RIP etc. Deep understanding of the mechanical behavior of SNF in transportation is crucial to prevent severe rod degradation.

In order to provide data on mechanical fatigue of SNF, the Cyclic Integrated Reversible-bending Fatigue Tester (CIRFT) has been developed by Oak Ridge Nuclear Laboratory [116]. Since its commissioning in 2013, SNF from various power plants have been studied with CIRFT. These include both BWRs and PWRs with different cladding materials (Zircaloy-2, Zircaloy-4, M5^{TM}) and with different

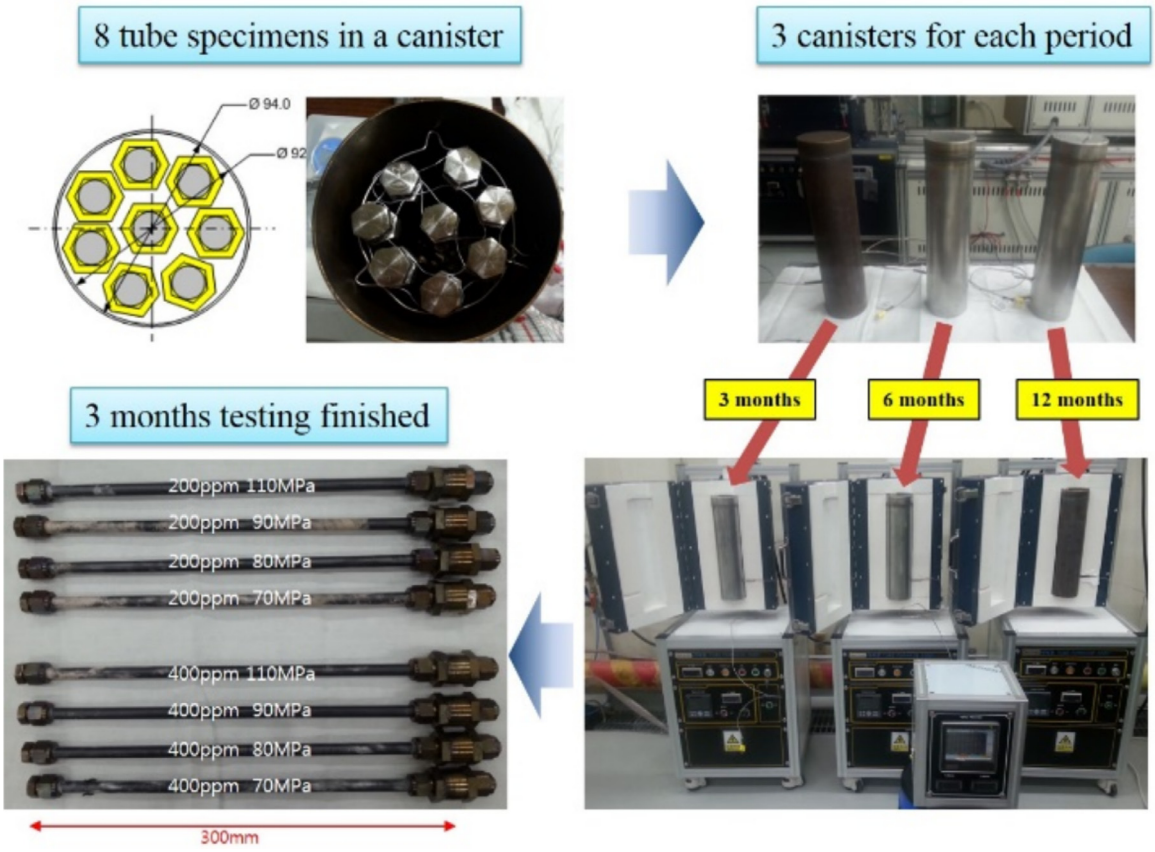

Fig. 25. KAERI's experimental setup for the low cooling rate experiments. Figure from Kook et al. [115].

fuels (UO_2, MOX)[117–119]. More recently, CIRFT's capabilities have been extended to allow studying hydride reorientation and annealing [120]. A comprehensive summary of the experiments carried out with CIRFT has been written by Wang et al. [106].

Among the important results obtained with CIRFT it is worth to mention these than can be studied with fuel performance codes or contribute to their development:

- cladding fatigue failures occur or are initiated mainly near the pellet-pellet interface,
- thick oxide layer and high hydrogen concentration can reduce rod fatigue time to failure,
- pellet-cladding and pellet-pellet bonding efficiency can significantly affect SNF fatigue time to failure by changing the rod flexural rigidity,
- stress concentrations and residual stresses in SNF strongly depend on the in-reactor stress history.

4.5. DEMO Project

High Burnup Nuclear Fuel Storage Demonstration project (DEMO) was proposed by DOE in 2013 [16]. DEMO is aimed at obtaining data on high burnup fuel behavior in dry storage conditions. In 2017, a TN32 storage cask was loaded with 32 fuel assemblies and installed at the North Anna Nuclear Generation Station. Four different cladding materials were used in these assemblies: Zircaloy-4, low tin Zircaloy-4, Zirlo and M5^{TM}. The range of burnups varies from 50.5 to 55.5 GWd/tU. The cask was modified to allow introducing several thermo-couples to monitor temperature at different locations inside the cask. The duration of the experimental storage period is planned to be 10 years.

In addition to the dry storage experiment, the sister rods have been selected and submitted to experimental examination. The sister rods have the same characteristic as the fuel rods loaded in the cask. The results obtained from the sister rods will be used to evaluate how the fuel state changes during 10 years of dry storage.

5. Multiphysics simulations of dry storage including fuel performance

Multiphysics computing environments aimed at studying behavior of nuclear reactors are being developed worldwide. Coupling of sophisticated thermo-hydraulics, neutronics or fuel performance codes can form together calculation chains that are necessary to account for the complex multiphysics taking place in the fuel during its entire life.

5.1. Generic scheme

Dry storage is usually preceded by base irradiation, wet storage and drying. It is important to properly model each stage of the life cycle since the state of the fuel and cladding at each stage depends largely on the previous one. Development of multiphysics couplings presented by different countries, that can be seen in Section 5.2, follows the same pattern. The authors model each stage of the fuel life cycle using dedicated tools and pass boundary conditions from one to another. In this paper, a generic calculation chain is divided into four main parts, see Fig. 26. First three of them are neutronics, thermo-hydraulics and fuel performance calculations. All these domains are crucial for predicting the fuel rod physical state. Although the fuel codes can do multiphysics to some extent, the idea is to use the strength of each code and couple them for high fidelity results. The enveloping element of the chain is the identification of the parameters having the biggest impact on the fuel rod integrity through sensitivity analysis.

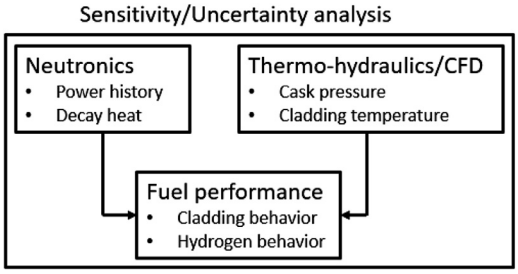

Fig. 26. A schematic representation of the multiphysics calculation chain.

5.1.1. Neutronics

Neutron transport and decay chains analyses are the first step in fuel performance modeling. One of the outputs from neutronics calculations is the generated heat. It gives the power distribution in the rod during in-reactor irradiation and the decay heat generated by fission products and actinides during storage [7]. Obtained radial heat generation can be used as the boundary condition for thermo-hydraulics and fuel performance computations.

Different sorts of codes can be used in the calculation chain for dry storage depending on what the author wants to achieve. The core-wide codes like Serpent [121] can provide detailed results of each stage of dry storage but using them is associated with long computing time. In turn, sometimes it is not necessary to carry out sophisticated neutronics computations and using a simpler neutronics module like ORIGEN [42] or TUBRNP [122] can be sufficient and much less time consuming.

5.1.2. Thermo-hydraulics/CFD

The heat generation within the fuel provided by the neutronics computations is used to calculate the cladding outer temperature. Different numerical tools can be used at different stages of the fuel cycle. Simple models incorporated in fuel performance codes can handle heat transfer between the cladding and the bulk of the coolant during in-reactor operation. The wet storage period is in general associated with a constant coolant temperature which can be directly imposed in the code. However, in dry storage, the decay heat from spent fuel assemblies is removed by gas like helium or nitrogen circulating naturally within the cask. Modeling such a natural circulation system requires dedicated thermo-hydraulics tools like COBRA-SFS [12] or advanced Computational Fluid Dynamics (CFD) software like FLUENT [123] or OpenFOAM [124].

5.1.3. Fuel performance

Fuel performance modeling is the central part of the calculation chain. There is a variety of codes available. In general, they are designed to study in-reactor conditions, either normal or accidental. However, these codes can be extended to dry storage by implementing relevant models like these described in Section 3.

Fuel behavior codes can use output parameters from neutronics and thermo-hydraulics simulations as boundary conditions for heat transfer calculations within the rod. Knowing the exact temperature distribution during dry storage is crucial since many parameters depend on it.

5.1.4. Uncertainties and sensitivity analysis

Each domain described above is associated with uncertainties. Coupling them leads to propagation of uncertainties. Moreover, trying to predict the fuel rod state decades or even hundreds of years ahead cannot be easily supported by experimental observations that would reduce uncertainties. Therefore, one has to rely on numerical simulations. To make them more reliable, it is necessary to identify the parameters having the biggest impact on the rod integrity and carry out a sensitivity analysis of them. The importance of sensitivity study led the authors of this review to consider it as a separate, fourth element of the calculation chain.

5.2. Multiphysics simulations in chosen countries

Multiple countries develop calculation chains to study dry storage. This subsection gives a short description of subjectively the most interesting programs, alphabetically sorted, launched by different countries. The calculations chains described in this section are listed in Table 8.

5.2.1. Finland

In Finland, the study on dry storage has been done in the frame of the Finnish Research Programme on Nuclear Power Plant Safety SAFIR2014 [125] and SAFIR2018 [126]. A calculation chain for the analysis of SNF under dry storage conditions in Finland has been done at the Research Center of Finland VTT and described by Arkoma et al. [15]. In the demonstration case, simulated by the authors, a CASTOR® V/21 cask is filled with 21 PWR fuel assemblies. The main characteristics of the fuel rod come from the BEAVRS benchmark specifications [127]. The parameters related to the cask are based on the EPRI technical report [128]. Arkoma et al. study the period of 300 years after discharge from the reactor.

The neutronics calculations have been done with the VTT's in-house code Serpent [121]. In the demonstration case, Serpent is used to perform burnup calculations during in-reactor irradiation until 50 GWd/tU, and then it provides decay heat for dry storage. The results obtained by Serpent are also used as the boundary conditions in CFD computations.

An open source package OpenFOAM has been used by Arkoma et al. to perform CFD analyses [124]. Convection, conduction and radiation are taken into account in the simulation. The rod external pressure during the wet and dry storage periods are not calculated by CFD in the demonstration case. The authors plan to fully couple the fuel performance and CFD codes for real scenarios. The wet storage temperature is constant and equal 50 °C. In the simulation, the wet storage duration was adjusted to obtain the maximum cladding temperature around 400 °C at the beginning of dry storage. The drying process preceding dry storage is not modeled for simplification.

The fuel performance modeling has been done with the VTT-ENIGMA code [129,130]. The main modification of the code done by Arkoma et al. was the implementation of the EDF and CIEMAT creep models dedicated for dry storage (see Section 3.4). Both models have been adjusted to fit the creep formalism of VTT-ENIGMA.

Arkoma et al. studied sensitivity of three parameters influencing the rod pressure: initial fill pressure, fission gas diffusion coefficient and power history. Randomly generated values of these variables have been obtained with Monte Carlo-type calculations. The authors carried out 5000 simulations per each creep model. The analysis has been done in the best-estimate manner with normal distribution.

The cladding creep hoop strains calculated with the EDF and CIEMAT models are shown in Fig. 27. One can see that generally, the EDF model gives higher values but the 5-95th curves from different models overlap and thus, it can be stated that the two models are consistent with each other. The cladding creep hoop strains calculated in the simulations are below the 1% safety criterion considered by Arkoma et al. The authors pointed that the maximum hoop stress obtained in the simulation is 74 MPa, which is in the vicinity of some hydride reorientation thresholds [131]. Thus, the fuel rods studied in the demonstration case could be susceptible to brittle failure.

Besides the Serpent–OpenFOAM–VTT-ENIGMA chain, Arkoma studied the same demonstration case with the fuel code BISON

Table 8
Multiphysics simulations of dry storage around the world.

Country	Institution	Neutronics	Thermo-hydraulics/CFD	Fuel code
Finland	VTT	Serpent	OpenFOAM	VTT-ENIGMA/BISON
Germany	GRS	KENOREST	COBRA-SFS	TESPA-ROD
Hungary	AEKI	ORIGEN	COBRA-SFS	TRANSURANUS
Russia	SRC RF TRINITI	-	RTEM-DS	RTOP-DS
Spain	CIEMAT	ORIGEN	FLUENT	FRAPCON
Switzerland	PSI	SNF	TRACE	Falcon
UK	NNL	CMS/FISPIN	FLUENT	NEXUS/ENIGMA
USA	DOE	MPACT	CTF/Star-CCM+	BISON

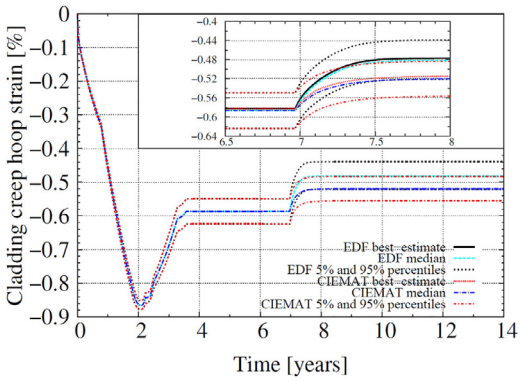

Fig. 27. Time evolution of the cladding creep hoop strain calculated with different models. Small figure shows the wet/dry storage transition. Figure from Arkoma et al. [15].

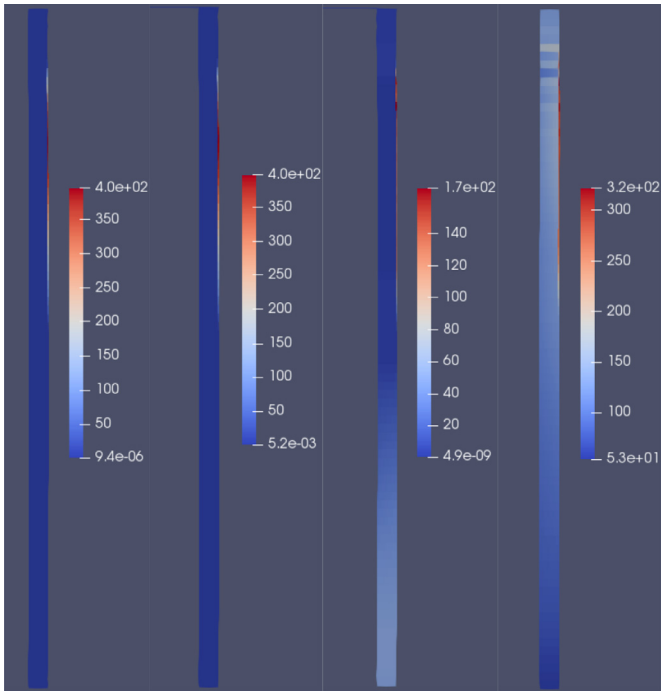

Fig. 28. Distribution of hydrides in the cladding calculated with BISON. From left to right, at the end of the base irradiation, during wet storage, at the beginning of dry storage, after 40 years. Figure from Arkoma [81].

[81]. Contrary to VTT-ENIGMA, BISON is able to carry out 2D simulations which are necessary to study hydrogen behavior in the cladding. BISON uses models for the hydrogen transport, dissolution and precipitation proposed by Courty et al. [74]. These models were previously described in Section 3.5.2. Fig. 28 presents the special distribution of hydrides at four different times during the fuel cycle from left to right: at the end of the base irradiation, during wet storage, and the beginning of dry storage and after 40 years. The calculation reproduces the experimentally observed tendency of the hydrides to gather near the cladding rim. Also, the highest concentrations occur in the upper part of the rod. It is associated with higher hydrogen uptake in that part.

5.2.2. Germany

Currently, the dry storage casks in Germany are licensed for 40 years. This period has to be extended since the final disposal facility will not be available before the license expiration. A new research program BREZL (German acronym for long term behavior of fuel assemblies at significantly longer interim storage) is ongoing at GRS to assess the fuel rod integrity during extended dry storage [132].

In the framework of BREZL, GRS has analyzed the temperature distribution in the storage cask using the code COBRA-SFS [12]. The neutronics calculations providing the power histories and decay heat have been carried out with KENOREST [133]. The fuel performance tool used in the dry storage simulations is the GRS's in-house code TESPA-ROD [54,134].

Several new models have been implemented into TESPA-ROD to extend its modeling capabilities to dry storage. Correlations for fuel swelling proposed by Raynaud and Einziger (see Section 3.1.3) has been added. The work of Raynaud and Einziger has also been used to derive a simple model for helium release [134]. It is correlated with the lattice swelling curves shown in Fig. 6.

New capabilities of TESPA-ROD also cover hydrogen behavior modeling. Boldt has implemented the hydrogen solubility and precipitation data and a criterion allowing to distinguish circumferential and radial hydrides [54], see Sections 3.1.2 and 3.5.3 respectively. Additionally, TESPA-ROD can predict the ductile-to-brittle transition with a model based on the work of Herb et al. [135].

Sonnenburg has published an example of the dry storage modeling done at GRS [134]. In the studied case, the author simulated the base irradiation, wet storage and dry storage of a fuel rod irradiated to 70 GWd/tU. Sonnenburg studied the impact of FGR on the gap size and the cladding hoop stress. The results are shown in Fig. 29.

5.2.3. Hungary

Literature review reveals that the very first multiphysics simulation focused on dry storage was done by the Hungarian Atomic Energy Research Institute AEKI at the beginning of the 21st century. The work of Gyori and Hozer concerned the Hungarian specific issue which was the storage of VVER fuel in Modular Vault Dry Storage (MVDS) [58].

Power histories for fuel performance and thermo-hydraulics calculations were provided by the neutronics code ORIGEN [42]. The thermo-hydraulics code COBRA-SFS [12] was applied to model the storage period. The fuel performance code used in the activity was TRANSURANUS [136]. Gyori and Hozer modified it by implementing the creep model proposed by Vesely et al. [57] (see

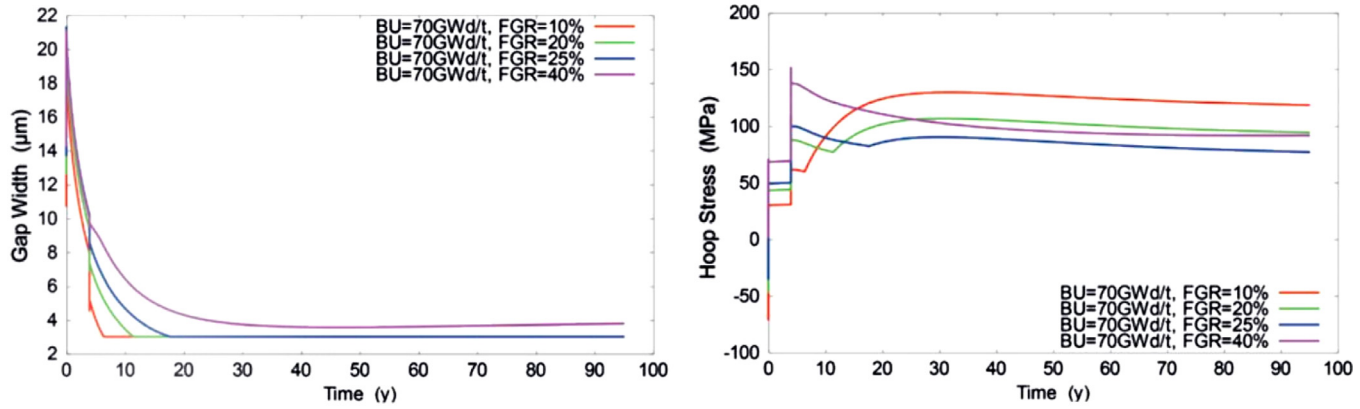

Fig. 29. Gap size (left figure) and hoop stress (right figure) evolution assuming different FGR fractions. Figure from Sonnenburg [134].

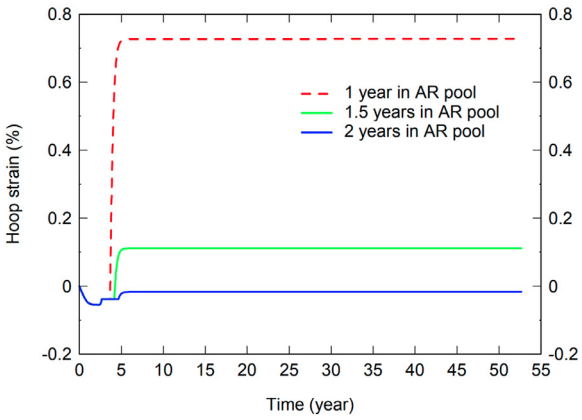

Fig. 30. Maximum residual hoop strain of the cladding calculated as a function of time. AR stands for 'At-Reactor'. Adapted from Gyori and Hozer [58].

Section 3.4.2). Even though the model is valid only for unirradiated Zr1Nb, the authors decided to use it to simulate irradiated claddings. This approach is conservative since the cladding material subjected to in-reactor irradiation has a lower ductility.

TRANSURANUS with the long-term creep model has been used to simulate scenarios consisting of base irradiation of a standard VVER-440 fuel rod, storage in the at-reactor pool and 50 years of dry storage in MVDS. The initial gap thickness used in the simulation has been maximized within the manufacture tolerance to maximize the FGR during base irradiation which increased RIP. This approach brings additional conservatism to the simulation. Three scenarios have been simulated. The difference between them is the cooling time in the at-reactor pool.

The results of the TRANSURANUS simulations are shown in Fig. 30. It presents the hoop strain time evolution. This parameters exhibits an expected behavior during base irradiation and wet storage. The strain change during dry storage, where the new creep model is applied, is visible only during the first months/years, and then it stabilizes at a constant value. This value strongly depends on the wet storage duration i.e. the cladding temperature. The hoop strain results presented by Gyori and Hozer have revealed how sensitive to the applied thermal boundary condition the cladding creep model is. In order to assess the impact of uncertainties of the cladding temperature, the authors have performed a probabilistic analysis.

The cladding temperature, calculated by COBRA-SFS, depends on several parameters. In the Monte Carlo analysis done by Gyori and Hozer, the authors assumed that these input parameters have a normal distribution of values with the 5% standard deviation. 500 Monte Carlo runs have been carried out for each parametric study in order to investigate the impact on the cladding mechanical response. The results of this analysis have revealed that a longer period of wet storage results in lower strains. Also, the 1% hoop strain safety margin can be exceeded if wet storage lasts one year.

5.2.4. Russia

Development of a software package for simulation of fuel behavior in dry storage is currently ongoing in Russia [137]. The software package consists of three main modules. First, the thermo-hydraulics module RTEM-DS is responsible for determining the fuel temperature during drying transportation and storage. Second, the fuel performance code RTOP-DS [138] is used to study fuel rod behavior including the phenomena shown schematically in Fig. 31. The last module is for a statistical analysis of obtained results.

The code RTOP-DS has several models developed to study dry storage. Among them is the creep model developed by Aliev et al. [110] (see Section 4.1) and a sophisticated hydrogen behavior model proposed by Kolesnik et al. [87] (see Section 3.5.3).

5.2.5. Spain

Numerical modeling of dry storage in Spain is very advanced. CIEMAT is the leader in this field. Work done by CIEMAT's researches cover thermo-hydraulics of storage casks, fuel performance modeling including development of new models and sophisticated sensitivity studies.

The thermal performance of storage casks has been studied by Herranz et al. [139]. The authors used the CFD code FLUENT [123] to perform 3D simulations of the HI-STORM 100s cask behavior in normal dry storage conditions. Then, the obtained results have been used by Feria et al. [140] to derive a correlation allowing to calculate the peak cladding temperature as a function of burnup and out-of-pile time. The burnup calculations used to derive the correlation have been done with the code ORIGEN [42]. This solution provides boundary conditions for fuel performance computations without coupling them to sophisticated CFD codes.

The fuel performance code used by CIEMAT is the in-house development of FRAPCON called FRAPCON-3xt [140]. Several models have been incorporated into this code to allow modeling of dry storage. Herranz and Feria have simplified the creep model developed by Bouffioux [59] and implemented it in FRAPCON [60]. The new model combines simplicity with high accuracy (see Section 3.4.4). Implementation of the model has been followed by the creep assessment of high burnup fuel rods [141]. The fuel performance modeling capabilities at CIEMAT account for hydrogen behavior models [84]. Feria and Herranz have implemented models for hydrogen precipitation, dissolution and two-phase diffusion. In addition, the authors considered the impact of the oxidation front on the hydrogen behavior. The most recent hydrogen-related development done by CIEMAT is the implementation of the hydride reorientation model derived by Desquines et al. [89]. Feria and

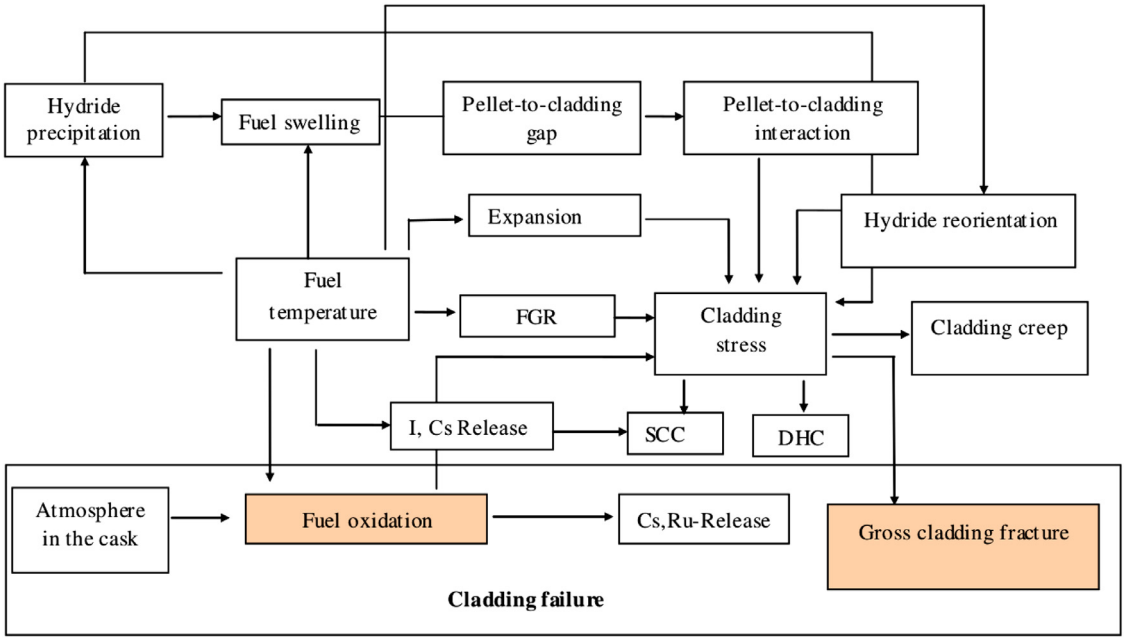

Fig. 31. Map of models used in the fuel behavior code RTOP-DS. Filled boxes indicate models under development. Figure adapted from Likhanskii et al. [137].

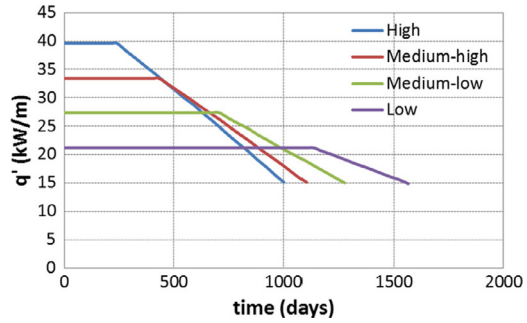

Fig. 32. Power histories used in the uncertainty study. Figure from Feria and Herranz [142].

Herranz integrated the model into the hydrogen behavior module of FRAPCON-3xt and applied it to four scenarii consisting of the base irradiation and 20 years of dry storage [53]. The authors have concluded that the precipitation of radial hydrides cannot be avoided if the fuel rod is at high temperature (400°C) and/or has a high burnup (62 GWd/tU).

The uncertainty study at CIEMAT has been done by Feria and Herranz [142]. The authors have used the Best Estimate Plus Uncertainty (BEPU) approach. Feria and Herranz have simulated four different cases. In each of them, a PWR rod is irradiated to 65 GWd/tU with different irradiation histories as shown in Fig. 32.

The four scenarios have been simulated with FRAPCON-3xt giving the best estimate results of the cladding hoop stress. The simulations take into account base irradiation, wet storage and dry storage. Once the best estimate results have been obtained, the toolkit DAKOTA [143] has been applied for uncertainty analyses. The uncertainties come from manufacturing parameters like the fuel rod dimensions and from used models like the FGR or cladding creep models. The results from the FRAPCON-3xt–DAKOTA uncertainty study are shown in Fig. 33.

The figure shows distributions of the cladding hoop stress for different power histories simulated by Feria and Herranz. The obtained results allowed the authors to derive burnup and temperature safety conditions for each power history.

5.2.6. Switzerland

STARS is the Swiss multiphysics environment developed at PSI. Recently, a subprogram of STARS [144] has been launched: DRYstars (DRY storage analyses for the reactors in switzerland) is aimed at extending the STARS modeling capabilities towards fuel safety analyses of Swiss operated fuel under dry storage conditions. The main tool used to simulate fuel integrity during an extended storage period is Falcon [49]. In the frame of DRYstars, Falcon's capabilities are being assessed and extended by implementing state-of-the-art models relevant for dry storage. The first development is the implementation of a creep model dedicated to dry storage conditions. The Falcon's default creep model, proposed by Limbäck and Anderson [145], fails to correctly predict the experiments representing dry storage conditions; therefore the creep model derived by Bouffioux (see Section 3.4.3) has been implemented in Falcon [146].

The computing capabilities of STARS has recently been presented by Rochman et al. [7]. The authors have developed a new method to calculate radiation quantities for Swiss SNF assemblies and criticality values for their handling and storage. Rochman et al. analyzed more than 6000 fuel assemblies from 34 reactor cycles. Their work shows a great potential for identifying edge cases and providing boundary conditions for fuel performance and thermo-hydraulics computations planned in the framework of DRYstars.

5.2.7. UK

The UK National Nuclear Laboratory (NNL) has developed the NEXUS code to automate fuel performance modeling of a whole LWR core [130]. NEXUS is coupled with a single rod behavior code ENIGMA [147] and uses it as the underlying fuel performance engine. Both codes are parts of the NNL's framework for dry storage modeling. The neutronics calculations are done by CMS and FISPIN [148]. The first one gives irradiation histories and the second one provides the decay heat and isotopic composition. The cladding outer temperatures during drying and dry storage can be calculated either by in-house codes or commercial software like FLUENT [123].

Rossiter has extended ENIGMA's capabilities to dry storage by introducing two significant modifications [130]. First, the out-of-pile creep model developed by Bouffioux has been implemented

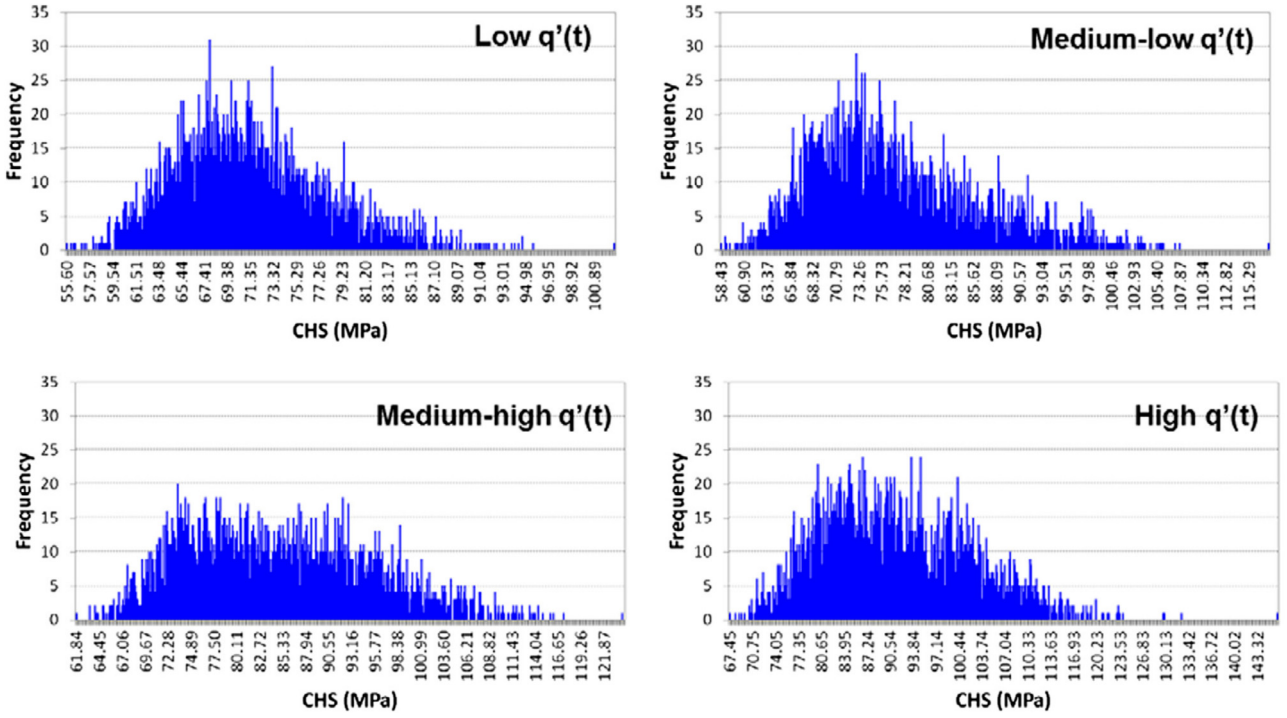

Fig. 33. Cladding hoop stress (CHS) distributions for each power history. Adapted from Feria and Herranz [142].

(see Section 3.4.3). Second, the cladding is assumed to be annealed instantaneously at the beginning of dry storage. This approach brings additional conservatism since the annealing removes the irradiation hardening effect. The main application of the extended ENIGMA is to predict if the rod integrity during storage is threatened by phenomena like the creep rupture or DHC. It is achieved by comparing the calculated values of the cladding temperature, hoop stress and hoop strain during drying and dry storage to the safety limits, typically, 370–570 °C, 90–120 MPa and 1% respectively [149].

The UK calculation chain has been applied to dry storage assessments for both UO_2 and MOX fuels with the dry storage period up to 100 years. An example of UO_2 irradiated to 47 GWd/tU has been presented by Rossiter [130]. The performed simulations accounts for base irradiation, wet storage and dry storage. The drying process has not been considered. The obtained results are presented in Fig. 34.

5.2.8. USA

The work done by Aly et al. for DOE [80] qualifies as a multiphysics simulation. The authors validate 3D fuel rod simulations by comparing the predicted hydrogen behavior results to experimental data. This work shows the coupling of BISON with the neutronics code MPACT [150] and the thermo-hydraulics code CTF and CFD code Star-CCM+ [151]. Sensitivity studies of numerous parameters are included. Even though the presented couplings and simulations do not concern dry storage conditions, they show a great potential for future developments concerning this domain.

6. International cooperation

6.1. Extended Storage Collaboration Program

The Extended Storage Collaboration Program (ESCP) was launched by EPRI in 2009 [152]. Several subcommittees have been established within ESCP. One of them is the International Subcommittee (IS) which gathers institutions from different countries and is focused on improving understanding of degradation mechanisms occurring during storage and transportation of SNF. Also, IS is responsible for expanding access to data and programs associated with SNF and for improving the overall technical basis. In 2012, IS released a report summarizing the status of SNF storage and providing a review of the technical data gaps in each of participant countries [153]. Regular meetings of IS are organized in the frame of ESCP. The most recent one took place in 2018 in Germany in conjunction with an international workshop held by GRS.

6.2. IAEA Coordinated Research Projects

IAEA has been leading Coordinated Research Projects (CRP) concerning extended storage of SNF since 1981 when the project BEhaviour of spent Fuel Assemblies during extended STorage (BEFAST) was launched. It was followed by the BEFAST-II and BEFAST-III. In 1997, IAEA launched the Spent fuel Performance Assessment and Research (SPAR) consisting of four phases: SPAR I, SPAR II, SPAR III and SPAR IV. The overall objective of the BEFAST and SPAR projects was to create a technical knowledge database on the SNF behavior and base it on operating experience and research activities performed by participating member states [154,155].

Another CRP proposed by IAEA is the DEMOnstrating performance of spent fuel and related storage system components during very long term storage (DEMO) launched in 2012 [156]. The main goals of DEMO were to exchange and share the knowledge on interim storage of SNF and to develop a network of experts in this field. The integrity and behavior of the fuel cladding in long term storage and the review of the past, currently ongoing and planned demonstration programs were among several technical areas considered in the project. The demonstration cases are being carried out by Japan, Korea and the U.S. All these experiments are promising in terms of obtaining new, valuable data to support modeling of dry storage.

As of today, a new CRP, Spent Fuel Research and Assessment (SFERA), is planned. Its objectives are similar to these of the BEFAST and SPAR projects, i.e, to continue developing a technical

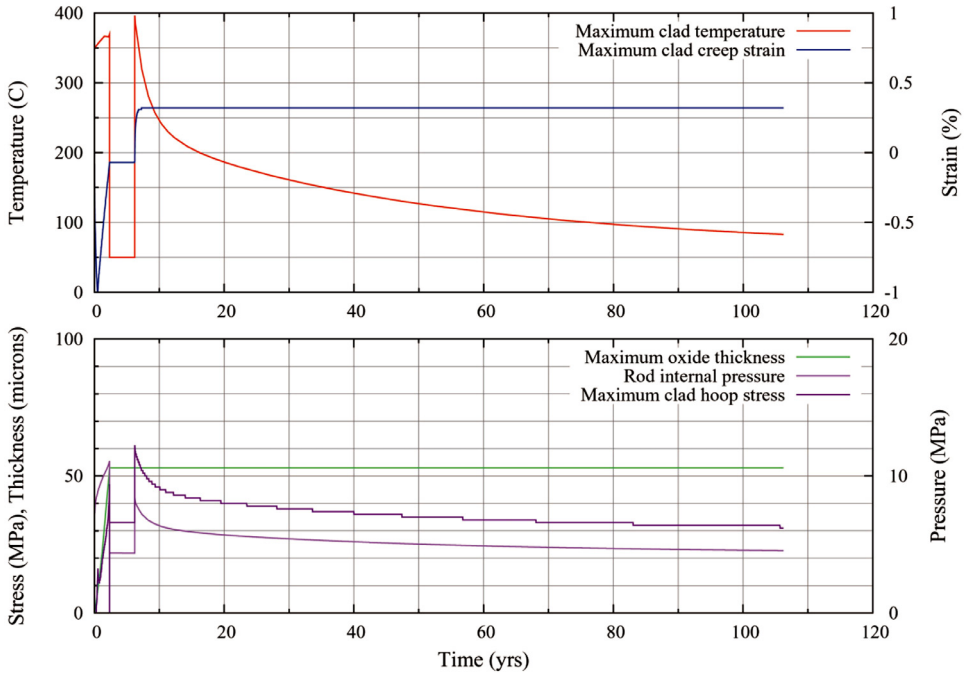

Fig. 34. An example of ENIGMA calculations. Figure from Rossiter [130].

knowledge database on the behavior of SNF and storage system materials.

6.3. GRS Benchmark for thermo-mechanical fuel rod behavior during dry storage

In 2019, GRS called a benchmark for thermo-mechanical fuel rod behavior during dry storage. The benchmark uses publicly available data and generic models. The simulated scenario consists of base irradiation, wet storage, drying and dry storage in a generic cask similar to CASTOR®V/19. The organizers have provided boundary conditions for fuel performance computations including the decay heat calculated with the code OREST [133] and the cladding outer temperature during drying and dry storage calculated with COBRA-SFS [12]. GRS provided boundary conditions for two cases: for the central and corner fuel rods of the central assembly in the cask. Simulations of these two fuel rods coated with Zircaloy-4 and M5^{TM} claddings have been requested which gives four cases overall.

7. Conclusions

In this paper, literature on the modeling of SNF in dry storage conditions has been reviewed with a focus on building a comprehensive overview of the current modeling trends. The main goal of this review is to present current activities related to fuel performance modeling in dry storage conditions.

During the drying process and subsequent dry storage of SNF, the fuel cladding is submitted to specific conditions like high temperature and high tensile stresses. The limits on these parameters have been defined by various countries to prevent cladding degradation and ensure rod integrity. Such limits as well as realistic storage conditions are given within this review.

Our review concludes that the main mechanisms for LWR fuel rod degradation in dry storage conditions are hydrogen-related effects and cladding creep. These mechanisms strongly depend on the distribution of stresses in the cladding, which are influenced by a variety of phenomena like the pellet-cladding bonding, fission gas release or fuel pellet swelling. The available models representing these mechanisms have been collected and described in this work.

In addition, current and planned experimental efforts supporting future dry storage modeling have been identified and reviewed. Recent experimental studies have revealed significantly different hydrogen behaviors in liner claddings compared to single-layered ones demonstrating the necessity of separate model development. Ongoing slow-cooling experiments with rates much slower than previous experiments appear especially valuable. Preliminary results of slow-cooling tests have already shown the significant effect of cooling rates on the cladding mechanical performance. Additionally, the experimental efforts towards better understanding the mechanical fatigue of SNF during transportation have been reviewed. It has been shown that the rod integrity in transportation strongly depends on burnup, oxide thickness and stress distribution. High fidelity estimations of such parameters can be obtained with fuel performance codes. Therefore, such modeling can be employed to study transportation issues in the future. Finally, new experimental data are expected to include long-term cladding creep essential for model validation.

Dry storage conditions can be simulated with a multiphysics simulation environment accounting for neutronics, thermo-hydraulics or CFD and fuel performance. Using dedicated codes for each of these domains may guarantee high fidelity results if sound validations have been performed. This is crucial in case of dry storage of SNF, as the long duration of such storage experiments is unrealistic. Computation chains developed by different countries are presented and their respective advancement is described. In general, the aim of multiphysics dry storage simulations is to verify whether the studied fuel rod fulfills the safety criteria. Typically, the maximum cladding hoop stress and strain and the maximum allowable temperature are of greatest concern.

Finally, several international programs focused on dry storage research have been described. Projects such as ESCP and IAEA CRPs focus on developing the network of experts and promoting international cooperation.

Declaration of Competing Interest

The authors declare that they have no known competing financial interests or personal relationships that could have appeared to influence the work reported in this paper.

CRediT authorship contribution statement

Piotr Konarski: Writing - original draft, Conceptualization. **Cédric Cozzo:** Writing - review & editing, Conceptualization, Supervision, Funding acquisition. **Grigori Khvostov:** Writing - review & editing, Funding acquisition. **Hakim Ferroukhi:** Writing - review & editing, Funding acquisition.

Acknowlgedgments

This literature review has been prepared in the frame of the DRYstars program, co-funded by PSI and the Swiss Federal Nuclear Safety Inspectorate ENSI.

The authors would like to thank A. Arkoma, F. Boldt, B. Chen, F. Feria, M. Li, Z. Li, P. Raynaud and A. Sasahara for sharing valuable information that allowed to improve this review.

References

[1] Storing spent fuel until transport to reprocessing or disposal, Report NF-T-3.3 in Nuclear Energy Series, Vienna: International Atomic Energy Agency. 2019
[2] C. Poinssot, P. Toulhoat, J.-M. Gras, P. Vitorge, Long term evolution of spent nuclear fuel in long term storage or geological disposal. new findings from the french PRECCI r&d program and implications for the definition of the RN source term in geological repository, J Nucl Sci Technol 39 (2014) 473–476, doi:10.1080/00223131.2002.10875509.
[3] P.V. Uffelen, J. Hales, W. Li, G. Rossiter, R. Williamson, A review of fuel performance modelling, J. Nucl. Mater. 516 (2019) 373–412, doi:10.1016/j.jnucmat.2018.12.037.
[4] T. Aliev, V. Likhanskii, I. Evdokimov, D. Ivonin, K. Mikhail, A. Sorokin, K. Ulibishev, V. Zborovskii, N. Elkin, M. Chernetsky, O. Khoruzhii, E. Zvir, P. Ilyin, B. Gurovich, O. Zabusov, V. Proselkov, Software package for safety analysis of dry storage regimes of spent russian nuclear fuel, in: XII Int. Conference on WWER Fuel Performance, Modelling and Experimental Support, 2017.
[5] L.I. Duarte, F. Fagnoni, R. Zubler, G. Weijia, P. Trtik, J. Bertsch, Hydrides in irradiated linear cladding–local and in-depth concentration determination by neutron radiography, in: Global 2019 / Top Fuel 2019 Conference, 2019.
[6] L.I. Duarte, F. Fagnoni, R. Zubler, G. Weijia, P. Trtik, J. Bertsch, Hydride characterization in Zircaloy-2 liner after C-shaped ring compression tests, in: Global 2019 / Top Fuel 2019 Conference, 2019.
[7] D. Rochman, A. Vasiliev, H. Ferroukhi, M. Pecchia, Consistent criticality and radiation studies of swiss spent nuclear fuel: the CS_2m approach, J. Hazard. Mater. 357 (2018) 384–392, doi:10.1016/j.jhazmat.2018.05.041.
[8] R.A. Lefebvre, P. Miller, J.M. Scaglione, K. Banerjee, J.L. Peterson, G. Radulescu, K.R. Robb, A.B. Thompson, H. Liljenfeldt, J.P. Lefebvre, Development of streamlined nuclear safety analysis tool for spent nuclear fuel applications, Nucl Technol 199 (3) (2017) 227–244, doi:10.1080/00295450.2017.1314747.
[9] J.B. Clarity, K. Banerjee, H.K. Liljenfeldt, W.J. Marshall, As-Loaded criticality margin assessment of dual-Purpose canisters using UNF-ST&DARDS, Nucl Technol 199 (3) (2017) 245–275, doi:10.1080/00295450.2017.1361250.
[10] G. Radulescu, K. Banerjee, R.A. Lefebvre, L.P. Miller, J.M. Scaglione, Shielding analysis capability of UNF-ST&DARDS, Nucl Technol 199 (3) (2017) 276–288, doi:10.1080/00295450.2017.1307643.
[11] K.R. Robb, J.M. Cuta, L.P. Miller, Thermal analysis capability of UNF-ST&DARDS, Nucl Technol 199 (3) (2017) 289–298, doi:10.1080/00295450.2017.1346446.
[12] T.E. Michener, D.R. Rector, J.M. Cuta, COBRA-SFS Thermal-Hydraulic analysis code for spent-Fuel storage and transportation casks: models and methods, Nucl Technol 199 (3) (2017) 330–349, doi:10.1080/00295450.2017.1305190.
[13] USNRC, Cladding considerations for the transportation and storage of spent fuel, ISG-11, Rev. 3 (2003).
[14] D. Kook, J. Choi, J. Kim, Y. Kim, Review of spent fuel integrity evaluation for dry storage, Nuclear engineering and technology 45 (1) (2013) 115–124.
[15] A. Arkoma, R. Huhtanen, J. Leppänen, J. Peltola, T. Pättikangas, Calculation chain for the analysis of spent nuclear fuel in long-term interim dry storage, Ann Nucl Energy 119 (2018) 129–138, doi:10.1016/j.anucene.2018.04.037.
[16] High Burnup Dry Storage Cask Research and Development Project Final Test Plan, EPRI, 2014, Contract No.: DE-NE-0000593.
[17] EPRI program 41.03.01: Used Fuel and High-Level Waste Management, https://www.epri.com/research/programs/061149/hbudemo.
[18] End-of-Life Rod Internal Pressures in Spent Pressurized Water Reactor Fuel, EPRI report 3002001949, 2013
[19] A. Motta, L. Capolungo, L. Chen, M. Cinbiz, M. Daymond, D. Koss, E. Lacroix, G. Pastore, P. Simon, M. Tonks, B. Wirth, M. Zikry, Hydrogen in zirconium alloys: a review, J. Nucl. Mater. 518 (2019) 440–460, doi:10.1016/j.jnucmat.2019.02.042.
[20] P. Bossis, D. Pêcheur, K. Hanifi, J. Thomazet, M. Blat, Comparison of the high burn-Up corrosion on M5 and low tin zircaloy-4, J. ASTM Int. 3 (1) (2006) 1–32, doi:10.1520/JAI12404.
[21] A. Couet, A.T. Motta, A. Ambard, The coupled current charge compensation model for zirconium alloy fuel cladding oxidation: i. parabolic oxidation of zirconium alloys, Corros Sci 100 (2015) 73–84, doi:10.1016/j.corsci.2015.07.003.
[22] B. Cox, Y.-M. Wong, A hydrogen uptake micro-mechanism for zr alloys, J. Nucl. Mater. 270 (1) (1999) 134–146, doi:10.1016/S0022-3115(98)00898-8.
[23] M. Veshchunov, A. Berdyshev, Modelling of hydrogen absorption by zirconium alloys during high temperature oxidation in steam, J. Nucl. Mater. 255 (2) (1998) 250–262, doi:10.1016/S0022-3115(98)00018-X.
[24] M. Tupin, F. Martin, C. Bisor, R. Verlet, P. Bossis, J. Chene, F. Jomard, P. Berger, S. Pascal, N. Nuns, Hydrogen diffusion process in the oxides formed on zirconium alloys during corrosion in pressurized water reactor conditions, Corros Sci 116 (2017) 1–13, doi:10.1016/j.corsci.2016.10.027.
[25] Identification and Prioritization of the Technical Information Needs Affecting Potential Regulation of Extended Storage and Transportation of Spent Nuclear FuelTechnical Report, U.S. NRC, 2014.
[26] Review of Used Nuclear Fuel Storage and Transportation Technical Gap AnalysesTechnical Report, U.S. Departament of Energy, 2012. FCRD-USED-2012-000215, PNNL-21596
[27] V. Rondinella, T. Wiss, D. Papaioannou, R. Nasyrow, D. Wegen, Nuclear fuel safety after discharge: Property evolution and testing, in: LWR Fuel Performance Meeting / Top Fuel 2013 Conference, 2013.
[28] P.A. Raynaud, R.E. Einziger, Cladding stress during extended storage of high burnup spent nuclear fuel, J. Nucl. Mater. 464 (2015) 304–312, doi:10.1016/j.jnucmat.2015.05.008.
[29] D. Baron, L. Hallstadius, 2.19 - Fuel Performance of Light Water Reactors (Uranium Oxide and MOX), in: R.J. Konings (Ed.), Comprehensive Nuclear Materials, Elsevier, Oxford, 2012, pp. 481–514, doi:10.1016/B978-0-08-056033-5.00040-9.
[30] L. Luzzi, L. Cognini, D. Pizzocri, T. Barani, G. Pastore, A. Schubert, T. Wiss, P.V. Uffelen, Helium diffusivity in oxide nuclear fuel: critical data analysis and new correlations, Nucl. Eng. Des. 330 (2018) 265–271, doi:10.1016/j.nucengdes.2018.01.044.
[31] L. Cognini, D. Pizzocri, T. Barani, P.V. Uffelen, A. Schubert, T. Wiss, L. Luzzi, Helium solubility in oxide nuclear fuel: derivation of new correlations for Henry's constant, Nucl. Eng. Des. 340 (2018) 240–244, doi:10.1016/j.nucengdes.2018.09.024.
[32] K. Hesketh, G. Rossiter, R. Largenton, M. Puide, 2.04 - Burnable Poison-Doped Fuel, in: R.J. Konings, R.E. Stoller (Eds.), Comprehensive Nuclear Materials (Second Edition), second edition, Elsevier, Oxford, 2020, pp. 106–124, doi:10.1016/B978-0-12-803581-8.11699-6.
[33] Z. Talip, T. Wiss, E.-A. Maugeri, J.-Y. Colle, P.-E. Raison, E. Gilabert, M. Ernstberger, D. Staicu, R. Konings, Helium behaviour in stoichiometric and hyperstoichiometric UO_2, J Eur Ceram Soc 34 (5) (2014) 1265–1277, doi:10.1016/j.jeurceramsoc.2013.11.032.
[34] F. Rufeh, D.R. Olander, T.H. Pigford, The solubility of helium in uranium dioxide, Nucl. Sci. Eng. 23 (4) (1965) 335–338, doi:10.13182/NSE65-A21069.
[35] E. Maugeri, T. Wiss, J.-P. Hiernaut, K. Desai, C. Thiriet, V. Rondinella, J.-Y. Colle, R. Konings, Helium solubility and behaviour in uranium dioxide, J. Nucl. Mater. 385 (2) (2009) 461–466, doi:10.1016/j.jnucmat.2008.12.033.
[36] K. Nakajima, H. Serizawa, N. Shirasu, Y. Haga, Y. Arai, The solubility and diffusion coefficient of helium in uranium dioxide, J. Nucl. Mater. 419 (1) (2011) 272–280, doi:10.1016/j.jnucmat.2011.08.045.
[37] G. Khvostov, K. Mikityuk, M. Zimmermann, A model for fission gas release and gaseous swelling of the uranium dioxide fuel coupled with the FALCON code, Nucl. Eng. Des. 241 (8) (2011) 2983–3007, doi:10.1016/j.nucengdes.2011.06.020.
[38] L. Verma, L. Noirot, P. Maugis, Modelling intra-granular bubble movement and fission gas release during post-irradiation annealing of UO_2 using a meso-scale and spatialized approach, J. Nucl. Mater. 528 (2020) 151874, doi:10.1016/j.jnucmat.2019.151874.
[39] USNRC, Cladding Stress during Extended Storage of High Burnup Spent Nuclear Fuel, Tech. rep. no. ML15180A411, 2015.
[40] K. Geelhood, W. Luscher, FRAPCON-3.5: Integral assessment, report no. NUREG/CR-7022, Vol. 2, Rev. 1 (2014).
[41] E.P. Simonen, E.R. Gilbert, DATING: A computer code for determining allowable temperatures for dry storage of spent fuel in inert and nitrogen gases, report no. PNL-6639, 1988.
[42] O. Gauld, R.W. Hermann, ORIGEN Scale System Module to Calculate Fuel Depletion, Actinide Transmutation, Fission Product Buildup and Decay, and Associated Radiation Terms, Technical Report, Oak Ridge National Laboratory, ORNL/TM-2005/39, Version 6, Vol. II, Sect. F7, 2005.
[43] J. Kim, H. Yoon, D. Kook, Y. Kim, A study on the initial characteristics of domestic spent nuclear fuels for long term dry storage, Nuclear Engineering and Technology 45 (3) (2013) 377–384, doi:10.5516/NET.06.2012.082.
[44] J.-S. Kim, J.-D. Hong, Y.-S. Yang, D.-H. Kook, Rod internal pressure of spent nuclear fuel and its effects on cladding degradation during dry storage, J. Nucl. Mater. 492 (2017) 253–259, doi:10.1016/j.jnucmat.2017.05.047.
[45] K. Geelhood, W. Luscher, P. Raynaud, I. Porter, FRAPCON-4.0: A Computer

Code for the Calculation of Steady-State, Thermal-Mechanical Behavior of Oxide Fuel Rods for High Burnup, Tech. rep., PNNL-19418, Vol.1 Rev.2. 2015
[46] R.N. Bratton, M.A. Jessee, W.A. Wieselquist, K.N. Ivanov, Rod internal pressure distribution and uncertainty analysis using frapcon, Nucl Technol 197 (1) (2017) 47–63, doi:10.13182/NT16-75.
[47] S. van den Berghe, A. Leenaers, B. Vos, L. Sannen, M. Verwerft, Observation of a pellet-cladding bonding layer in high power fuel, Technical Report, IAEA, 2004. IAEA-TECDOC–1416
[48] R. Williamson, J. Hales, S. Novascone, M. Tonks, D. Gaston, C. Permann, D. Andrs, R. Martineau, Multidimensional multiphysics simulation of nuclear fuel behavior, J. Nucl. Mater. 423 (1) (2012) 149–163, doi:10.1016/j.jnucmat.2012.01.012.
[49] M. Pytel, Falcon Fuel Performance Code Version 1.4.0: Verification and Validation Summary, Report No. 3002010719, EPRI, 2018, (0000).
[50] Impact of Fuel-Cladding Bonding on the Response of High-Burnup Spent PWR Fuel Subjected to Dry Storage and Transportation Accidents, Report No. 3002015075, EPRI, 2019
[51] M. Cunningham, E. Simonen, R. Allemann, I. Levy, R. Hazelton, E. Gilbert, Control of degradation of spent LWR fuel during dry storage in an inert atmosphere, PNL-6364, Pacific National Laboratory (1987).
[52] R.E. Einziger, H. Tsai, M.C. Billone, B. Hilton, Examination of spent PWR fuel rods after 15 years in dry storage, report no. NUREG/CR-6831 (2003).
[53] F. Feria, C. Aguado, L. Herranz, Extension of FRAPCON-xt to hydride radial reorientation in dry storage, Ann Nucl Energy 145 (2020) 107559, doi:10.1016/j.anucene.2020.107559.
[54] F. Boldt, Implementation of hydrogen solid solubility data and precipitation threshold stresses in the fuel rod code TESPA-ROD, Journal of Nuclear Engineering and Radiation Science 5 (2) (2019) 020904, doi:10.1115/1.4042118.
[55] B.A. Chin, M.A. Khan, J.C.L. Tarn, Deformation and fracture map methodology for predicting cladding behavior during dry storage, report PNL-5998 (1986).
[56] E.R. Gilbert, E.P. Simonen, C.E. Beyer, P.G. Medvedev, Update of CSFM methodology for determining temperature limits for spent fuel dry storage in inert gas, report ML022250067, PNNL (2001).
[57] J. Vesely, M. Valach, Z. Frejtich, V. Priman, Creep properties of unirradiated Zr1Nb nuclear fuel cladding tubes under normal and abnormal dry storage conditions, in: Storage of spent fuel from power reactors, Proceedings of a symposium held in Vienna, IAEA Document No. IAEA-SM-352/38, 1998.
[58] C. Gyori, Z. Hozer, TRANSURANUS simulation of WWER cladding creep under dry storage conditions, (IAEA-CN–102), in: International Conference on Storage of Spent Fuel from Power Reactors, Book of Extended Synopses, 2003. IAEA
[59] P. Bouffioux, Transportation and interim storage of PWR's spent fuel., Technical Report, EDF, HT25-C2005-192/PBF, 2005.
[60] L. Herranz, F. Feria, Extension of the FRAPCON-3.3 creep model to dry storage conditions, Prog. Nucl. Energy 52 (7) (2010) 634–639, doi:10.1016/j.pnucene.2010.04.003.
[61] G.A. Berna, G.A. Beyer, K.L. Davis, D.D. Lanning, FRAPCON-3: A computer code for the calculation of steady-state, thermal-mechanical behavior of oxide fuel rods for high burnup, 1997Tech. rep., NUREG/CR-6534-Vol.2. 10.2172/576110
[62] P. Kaufholz, M. Stuke, F. Boldt, M. Péridis, Influence of kinetic effects on terminal solid solubility of hydrogen in zirconium alloys, J. Nucl. Mater. 510 (2018) 277–281, doi:10.1016/j.jnucmat.2018.08.011.
[63] M.P. Puls, The effect of hydrogen and hydrides on the integrity of zirconium alloy components: Delayed hydride cracking, Springer Science & Business Media, 2012.
[64] A. Barrow, C. Toffolon-Masclet, J. Almer, M. Daymond, The role of chemical free energy and elastic strain in the nucleation of zirconium hydride, J. Nucl. Mater. 441 (1) (2013) 395–401, doi:10.1016/j.jnucmat.2013.06.013.
[65] O. Zanellato, M. Preuss, J.-Y. Buffiere, F. Ribeiro, A. Steuwer, J. Desquines, J. Andrieux, B. Krebs, Synchrotron diffraction study of dissolution and precipitation kinetics of hydrides in zircaloy-4, J. Nucl. Mater. 420 (1) (2012) 537–547, doi:10.1016/j.jnucmat.2011.11.009.
[66] Z. Pan, I. Ritchie, M. Puls, The terminal solid solubility of hydrogen and deuterium in zr-2.5Nb alloys, J. Nucl. Mater. 228 (2) (1996) 227–237, doi:10.1016/S0022-3115(95)00217-0.
[67] K. Une, S. Ishimoto, Y. Etoh, K. Ito, K. Ogata, T. Baba, K. Kamimura, Y. Kobayashi, The terminal solid solubility of hydrogen in irradiated zircaloy-2 and microscopic modeling of hydride behavior, J. Nucl. Mater. 389 (1) (2009) 127–136, doi:10.1016/j.jnucmat.2009.01.017.
[68] A. McMinn, E.C. Darby, J.S. Schofield, The terminal solid solubility of hydrogen in zirconium alloys, in: G.P. Sabol, G.D. Moan (Eds.), Zirconium in the Nuclear Industry: Twelfth International Symposium, ASTM International, STP1354, 2000, pp. 173–195.
[69] K. Colas, Fundamental Experiments on Hydride Reorientation in Zircaloy, The Pennsylvania State University, 2012 Ph.D. thesis.
[70] G. Marino, Hydrogen supercharging in zircaloy, Materials Science and Engineering 7 (6) (1971) 335–341, doi:10.1016/0025-5416(71)90016-4.
[71] B. Kammenzind, D. Franklin, W. Duffin, H. Peters, Hydrogen pickup and redistribution in alpha-annealed zircaloy-4, ASTM Spec. Tech. Publ. 1295 (1996), doi:10.2172/10181237.
[72] K. Une, S. Ishimoto, Dissolution and precipitation behavior of hydrides in zircaloy-2 and high Fe zircaloy, J. Nucl. Mater. 322 (1) (2003) 66–72, doi:10.1016/S0022-3115(03)00320-9.
[73] E. Lacroix, P.-C. Simon, A. Motta, J. Almer, Zirconium Hydride Precipitation and Dissolution kinetics in Zirconium Alloys, presented at the ASTM 19th International Symposium on Zirconium in the Nuclear Industry, Manchester, UK, 2019
[74] O. Courty, A.T. Motta, J.D. Hales, Modeling and simulation of hydrogen behavior in zircaloy-4 fuel cladding, J. Nucl. Mater. 452 (1) (2014) 311–320, doi:10.1016/j.jnucmat.2014.05.013.
[75] F. Passelaigue, E. Lacroix, G. Pastore, A.T. Motta, Implementation and validation of the hydride nucleation-Growth-Dissolution (HNGD) model in BISON, J. Nucl. Mater. (2020) 152683, doi:10.1016/j.jnucmat.2020.152683.
[76] J. Kearns, Diffusion coefficient of hydrogen in alpha zirconium, zircaloy-2 and zircaloy-4, J. Nucl. Mater. 43 (3) (1972) 330–338, doi:10.1016/0022-3115(72)90065-7.
[77] S.D. Harkness, W.A. Young, Diffusion coefficient of hydrogen in delta-phase zirconium hydride, Technical Report, 1965.
[78] A. Sawatzky, Hydrogen in zircaloy-2: its distribution and heat of transport, J. Nucl. Mater. 2 (4) (1960) 321–328, doi:10.1016/0022-3115(60)90004-0.
[79] H.S. Hong, S.J. Kim, K.S. Lee, Thermotransport of hydrogen in zircaloy-4 and modified zircaloy-4, J. Nucl. Mater. 257 (1) (1998) 15–20, doi:10.1016/S0022-3115(98)00430-9.
[80] A. Aly, M. Avramova, K. Ivanov, A. Motta, E. Lacroix, A. Manera, D. Walter, R. Williamson, K. Gamble, Three-dimensional fuel pin model validation by prediction of hydrogen distribution in cladding and comparison with experiment, Tech. rep., DOE NEUP Project 13–5180, 2017. 10.2172/1410438
[81] A. Arkoma, Modelling cladding hydrides in interim dry storage, Technical Report, VTT, VTT-R-05604-18, 2018.
[82] D. Stafford, Multidimensional simulations of hydrides during fuel rod lifecycle, J. Nucl. Mater. 466 (2015) 362–372, doi:10.1016/j.jnucmat.2015.06.037.
[83] M. Veshchunov, V. Shestak, V. Ozrin, A new model of hydrogen redistribution in zr alloy claddings during waterside corrosion in a temperature gradient, J. Nucl. Mater. 472 (2016) 65–75, doi:10.1016/j.jnucmat.2016.01.032.
[84] F. Feria, L. Herranz, Effect of the oxidation front penetration on in-clad hydrogen migration, J. Nucl. Mater. 500 (2018) 349–360, doi:10.1016/j.jnucmat.2018.01.011.
[85] M. Tupin, C. Bisor, P. Bossis, J. Chêne, J. Bechade, F. Jomard, Mechanism of corrosion of zirconium hydride and impact of precipitated hydrides on the zircaloy-4 corrosion behaviour, Corros Sci 98 (2015) 478–493, doi:10.1016/j.corsci.2015.05.058.
[86] H. Chu, S. Wu, R. Kuo, Hydride reorientation in zircaloy-4 cladding, J. Nucl. Mater. 373 (1) (2008) 319–327, doi:10.1016/j.jnucmat.2007.06.012.
[87] M. Kolesnik, T. Aliev, V. Likhanskii, Modeling of hydrogen behavior in spent fuel claddings during dry storage, J. Nucl. Mater. 508 (2018) 567–573, doi:10.1016/j.jnucmat.2018.06.012.
[88] G.V. Kulakov, A.V. Vatulin, Y.V. Konovalov, A.A. Kosaurov, M.M. Peregud, E.A. Korotchenko, V.Y. Shishin, A.A. Shel'dyakov, Analysis of the effect of the stress-strain state of irradiated zirconium-alloy fuel-element cladding on hydride orientation, At. Energy 122 (2) (2017) 87–92, doi:10.1007/s10512-017-0240-1.
[89] J. Desquines, D. Drouan, M. Billone, M. Puls, P. March, S. Fourgeaud, C. Getrey, V. Elbaz, M. Philippe, Influence of temperature and hydrogen content on stress-induced radial hydride precipitation in zircaloy-4 cladding, J. Nucl. Mater. 453 (1) (2014) 131–150, doi:10.1016/j.jnucmat.2014.06.049.
[90] K. Colas, A. Motta, M.R. Daymond, J. Almer, Mechanisms of Hydride Reorientation in Zircaloy-4 Studied in Situ, in: B. Comstock, P. Barberis (Eds.), Zirconium in the Nuclear Industry: 17th Volume, ASTM International, STP1543, 2015, pp. 1–31, doi:10.1520/STP154320120168.
[91] M.N. Cinbiz, A.T. Motta, D. Koss, M. Billone, Hydride Reorientation in Zircaloy-4 under Different States of Stress as Studied with In Situ X-Ray Diffraction, in: R. Comstock, A. Motta (Eds.), Zirconium in the Nuclear Industry: 18th International Symposium, ASTM International, STP1597, 2018, pp. 1252–1285, doi:10.1520/STP159720160052.
[92] R. Dutton, K. Nuttall, M. Puls, L. Simpson, Mechanisms of hydrogen induced delayed cracking in hydride forming materials., Metall Trans A 8 A (10) (1977) 1553–1562, doi:10.1007/BF02644858.
[93] K.B. Sorenson, B. Hanson, Making the case for safe storage of used nuclear fuel for extended periods of time: combining near-term experiments and analyses with longer-term confirmatory demonstrations, Nuclear Engineering and Technology 45 (4) (2013) 421–426, doi:10.5516/NET.06.2013.707.
[94] K. Chan, An assessment of delayed hydride cracking in zirconium alloy cladding tubes under stress transients, Int. Mater. Rev. 58 (2013) 349–373, doi:10.1179/1743280412Y.0000000013.
[95] V. Markelov, N. Saburov, S. Bekrenev, V. Novikov, Determination of thershold stress intensity factor, K_{IH}, in DHC tests of fuel claddings by method of constant displacement, TopFuel, Zurich, Switzerland, 2015.
[96] C. Coleman, V. Inozemtsev, V. Markelov, R. Roth, A.-M. Alvare-Holston, L. Ramanathan, Z. He, J.K. Chakravartty, V. Makarevicius, L. Ali, The Threshold Stress-Intensity Factor, K_{IH}, for Delayed Hydride Cracking (DHC) in Zircaloy-4 Fuel Cladding an IAEA Coordinated Research Project (CRP), WRFPM 2014, Sendai, Japan, 2014.
[97] S.-Q. Shi, M.P. Puls, Dependence of the threshold stress intensity factor on hydrogen concentration during delayed hydride cracking in zirconium alloys, J. Nucl. Mater. 218 (1) (1995) 30–36, doi:10.1016/0022-3115(94)00368-8.
[98] S. Suman, M.K. Khan, M. Pathak, R. Singh, 3D Simulation of hydride-assisted crack propagation in zircaloy-4 using XFEM, Int J Hydrogen Energy 42 (29) (2017) 18668–18673, doi:10.1016/j.ijhydene.2017.04.163. Special Issue on The 5th International Conference on Energy Engineering and Environmental Engineering (ICEEEE2017), 15–16 April 2017, Xiamen, China

[99] S. Suman, M.K. Khan, M. Pathak, R. Singh, et al., Effects of hydride on crack propagation in zircaloy-4, Procedia Eng 173 (2017) 1185–1190.
[100] Z. Xia, J. Zhang, Q. Tong, S. Ding, Multi-physics modeling of delayed hydride cracking in zirconium alloys, J Mech Phys Solids 132 (2019) 103677, doi:10.1016/j.jmps.2019.07.020.
[101] Y. Zhang, C. Jiang, X. Bai, Anisotropic hydrogen diffusion in α-zr and zircaloy predicted by accelerated kinetic monte carlo simulations, Sci Rep 7 (1) (2017) 41033, doi:10.1038/srep41033.
[102] S. Ishioka, M. Koiwa, Diffusion coefficient in crystals with multiple jump frequencies, Philos. Mag. A 52 (2) (1985) 267–277, doi:10.1080/01418618508237623.
[103] M. Liyanage, R. Miller, R.K.N.D. Rajapakse, Effect of Oxygen on Hydrogen Diffusivity in hcp-Zirconium, Available at arXiv:1909.02486, 2019.
[104] S.-Q. Shi, Z. Xiao, A quantitative phase field model for hydride precipitation in zirconium alloys: part i. development of quantitative free energy functional, J. Nucl. Mater. 459 (2015) 323–329, doi:10.1016/j.jnucmat.2014.03.013.
[105] Z. Xiao, M. Hao, X. Guo, G. Tang, S.-Q. Shi, A quantitative phase field model for hydride precipitation in zirconium alloys: part II. modeling of temperature dependent hydride precipitation, J. Nucl. Mater. 459 (2015) 330–338, doi:10.1016/j.jnucmat.2014.12.110.
[106] J.-A. Wang, H. Wang, H. Jiang, B. Bevard, High burn-up spent nuclear fuel transport reliability investigation, Nucl. Eng. Des. 330 (2018) 497–515, doi:10.1016/j.nucengdes.2018.02.007.
[107] B. Almomani, D. Jang, S. Lee, Structural integrity of a high-burnup spent fuel rod under drop impact considering pellet-clad interfacial bonding influence, Nucl. Eng. Des. 337 (2018) 324–340, doi:10.1016/j.nucengdes.2018.07.024.
[108] B. Almomani, S. Kim, D. Jang, S. Lee, Parametric study on the structural response of a high burnup spent nuclear fuel rod under drop impact considering post-irradiated fuel conditions, Nuclear Engineering and Technology 52 (5) (2020) 1079–1092, doi:10.1016/j.net.2019.10.022.
[109] H. Jiang, J.-A.J. Wang, H. Wang, The impact of interface bonding efficiency on high-burnup spent nuclear fuel dynamic performance, Nucl. Eng. Des. 309 (2016) 40–52, doi:10.1016/j.nucengdes.2016.09.013.
[110] T. Aliev, I. Evdokimov, V. Likhanskii, A. Sorokin, M. Kolesnik, A. Kozhakin, V. Zborovskii, E. Zvir, P. Ilyin, Modeling of Dimensional Changes of Spent WWER Fuel Rods during Dry Storage, in: 11th International Conference <<WER Fuel Performance: Modelling and Experimental Support>>, 2015.
[111] W. Gong, P. Trtik, A. Colldeweih, L. Duarte, M. Grosse, E. Lehmann, J. Bertsch, Hydrogen diffusion and precipitation in duplex zirconium nuclear fuel cladding quantified by high-resolution neutron imaging, J. Nucl. Mater. 526 (2019) 151757, doi:10.1016/j.jnucmat.2019.151757.
[112] P. Trtik, Neutron microtomography of voids in gold, MethodsX 4 (2017) 492–497, doi:10.1016/j.mex.2017.11.009.
[113] P. Trtik, E.H. Lehmann, Progress in high-resolution neutron imaging at the paul scherrer institut - the neutron microscope project, J. Phys. Conf. Ser. 746 (2016) 012004, doi:10.1088/1742-6596/746/1/012004.
[114] FuelSolutions, FuelSolutions W21 Canister Storage Final Safety Analysis Report Revision 5, Technical Report, 2007. Document No. WSNF-221
[115] D. Kook, J.H. Yang, Y.-H. Koo, Spent nuclear fuel integrity R&D work for dry storage in Korea, in: International High-Level Radioactive Waste Management Conference, Knoxville, USA, 2019.
[116] J.-A. Wang, H. Wang, B.B. Bevard, R.L. Howard, M.E. Flanagan, Reversal bending fatigue test system for investigating vibration integrity of spent nuclear fuel during transportation, Packaging, Transport, Storage & Security of Radioactive Material 25 (3–4) (2014) 119–132, doi:10.1179/1746510915Y.0000000002.
[117] J.-A. Wang, H. Wang, The Development of Reversible Bending Fatigue Tester and Its Application to High Burn-up Spent Nuclear Fuel Integrity Study under Normal Transportation Vibration, 2014. Tech. rep. ORNL/TM-2013/573
[118] J.-A. Wang, H. Wang, H. Jiang, B. Bevard, R. Howard, FY14 Status Report: Cirft Testing Results on High Burnup UNF, 2014. Tech. rep. ORNL/TM-2014/310
[119] J.-A. Wang, H. Wang, H. Jiang, Y. Yan, FY 2015 Status Report: Cirft Testing of High-Burnup Used Nuclear Fuel Rods from Pressurized Water Reactor and. Boiling Water Reactor Environments, 2015. Tech. rep. ORNL/TM-2015/313
[120] J.-A. Wang, H. Wang, Y. Yan, ORNL Interim Progress Report on Hydride Reorientation CIRFT Tests, 2015. Tech. rep. ORNL/TM-2016/660
[121] J. Leppänen, M. Pusa, T. Viitanen, V. Valtavirta, T. Kaltiaisenaho, The serpent monte carlo code: status, development and applications in 2013, Ann Nucl Energy 82 (2015) 142–150, doi:10.1016/j.anucene.2014.08.024.
[122] K. Lassmann, C. O'Carroll, J. van de Laar, C. Walker, The radial distribution of plutonium in high burnup UO_2 fuels, J. Nucl. Mater. 208 (3) (1994) 223–231, doi:10.1016/0022-3115(94)90331-X.
[123] Ansys Fluent, visited Apr. 9, 2021https://www.ansys.com/products/fluids/ansys-fluent.
[124] OpenFOAM Fundation, visited Apr. 9, 2021https://www.openfoam.com/.
[125] SAFIR2014, The Finnish Research Programme on Nuclear Power Plant Safety 2011 - 2014, visited Apr. 9, 2021http://safir2014.vtt.fi/index.htm.
[126] SAFIR2018, The Finnish Research Programme on Nuclear Power Plant Safety 2015 - 2018, visited Apr. 9, 2021http://safir2018.vtt.fi/.
[127] N. Horelik, B. Herman, B. Forget, K. Smith, Benchmark for evaluation and validation of reactor simulations (BEAVRS), v1. 0.1, in: Proc. Int. Conf. Mathematics and Computational Methods Applied to Nuc. Sci. & Eng, 2013, pp. 5–9.
[128] D. Dziadosz, E. Moore, J. Creer, R. McCann, M. McKinnon, J. Tanner, E. Gilbert, R. Goodman, D. Schoonen, M. Jensen, The CASTOR-V/21 PWR spent-fuel storage cask: Testing and analyses: Interim report, Technical Report, 1986. EPRI-NP-4887; PNL-5917
[129] S. Kelppe, K. Ranta-Puska, Calibration of the ENIGMA code for Finnish reactor fuel with support from experimental irradiations, IAEA report XA9744790, 1997.
[130] G. Rossiter, Development of the ENIGMA fuel performance code for whole core analysis and dry storage assessments, Nuclear Engineering and Technology 43 (6) (2011) 489–498.
[131] R.S. Daum, S. Majumdar, Y. Liu, M.C. Billone, Radial-hydride embrittlement of high-burnup zircaloy-4 fuel cladding, J Nucl Sci Technol 43 (9) (2006) 1054–1067, doi:10.1080/18811248.2006.9711195.
[132] F. Boldt, P. Kaufholz, M. Péridis, H.G. Sonnenburg, M. Stuke, Research activities at GRS on fuel rod behaviour during extended dry storage, Kerntechnik 83 (6) (2018) 476–483, doi:10.3139/124.110950.
[133] U. Hesse, S. Langenbuch, W. Zwermann, Nuclear codes and data libraries at GRS for reactivity and nuclide inventory calculations, in: The Eurosafe Forum 2003, 2003, p. 710.
[134] H.G. Sonnenburg, TESPA-ROD Code prediction of the fuel rod behaviour during long-term storage, International Journal for Nuclear Power 6/7 (2018).
[135] J. Herb, J. Sievers, H.-G. Sonnenburg, A new cladding embrittlement criterion derived from ring compression tests, Nucl. Eng. Des. 273 (2014) 615–630, doi:10.1016/j.nucengdes.2014.03.047.
[136] K. Lassmann, Transuranus: a fuel rod analysis code ready for use, J. Nucl. Mater. 188 (1992) 295–302, doi:10.1016/0022-3115(92)90487-6.
[137] V. Likhanskii, T. Aliev, M.Y. Kolesnik, I. Evdokimov, D. Ivonin, A. Sorokin, K. Ulibishev, V. Zborovskii, E. Zvir, P. Ilyin, A. Dolgov, A. Ugryumov, A. Shihkin, B. Gurovich, O. Zabusov, V. Proselkov, A. Frolov, Development of software package to justify safe dry storage of russian nuclear fuel, in: Proceedings of WRFPM 2017, Jeju Island, Republic of Korea, 2017. September 10, - 14
[138] V. Likhanskii, I. Evdokimov, A. Sorokin, V. Zborovskii, K. Ulybyshev, A. Burtsev, I. Goryushin, A. Ponomarev, A. Ugrumov, A. Shishkin, Codes and software in support of fuel operation in lwrs, LWR Fuel Performance Meeting, Top Fuel 2013 1 (2013) 203–210.
[139] L.E. Herranz, J. Penalva, F. Feria, CFD Analysis of a cask for spent fuel dry storage: model fundamentals and sensitivity studies, Annals of InProceedingsNuclear Energy 76 (2015) 54–62, doi:10.1016/j.anucene.2014.09.032.
[140] F. Feria, L. Herranz, J. Penalva, On the way to enabling FRAPCON-3 to model spent fuel under dry storage conditions: the thermal evolution, Ann Nucl Energy 85 (2015) 995–1002, doi:10.1016/j.anucene.2015.07.017.
[141] F. Feria, L. Herranz, Creep assessment of zry-4 cladded high burnup fuel under dry storage, Prog. Nucl. Energy 53 (4) (2011) 395–400, doi:10.1016/j.pnucene.2011.01.012.
[142] F. Feria, L. Herranz, Application of the BEPU methodology to assess fuel performance in dry storage, Ann Nucl Energy 99 (2017) 240–246, doi:10.1016/j.anucene.2016.08.029.
[143] M. Eldred, K. Dalbey, W. Bohnhoff, B. Adams, L. Swiler, P. Hough, D. Gay, J. Eddy, K. Haskell, DAKOTA: A Multilevel Parallel Object-oriented Framework for Design Optimization, Parameter Estimation, Uncertainty Quantification, and Sensitivity Analysis. Version 5.0, User's Manual, 2009, doi:10.2172/991842.
[144] STARS Program https://www.psi.ch/de/stars.
[145] M. Limbäck, T. Andersson, A Model for Analysis of the Effect of Final Annealing on the In- and Out-of-Reactor Creep Behavior of Zircaloy Cladding, ASTM International, West Conshohocken, PA, pp. 448–468. STP1295. 10.1520/STP16185S
[146] P. Konarski, C. Cozzo, G. Khvostov, H. Ferroukhi, Dry storage modeling activities at PSI: implementation and testing of a creep model for dry storage, Kerntechnik 85 (6) (2020) 419–425, doi:10.3139/124.200072.
[147] P.A. Jackson, J.A. Turnbull, R.J. White, A description of the ENIGMA Fuel Performance Code, IAEA Technical Committee Meeting on Water Reactor Fuel Element Computer Modelling in Steady-State, Transient and Accident Conditions, Preston, UK, 1988.
[148] D.R. Parker, R.W. Mills, FISPIN10 Validation Review, Report RAT 1972 Issue 02, 2001.
[149] H.-G. Kim, Y.-H. Jeong, K.-T. Kim, The effects of creep and hydride on spent fuel integrity during interim dry storage, Nuclear engineering and technology 42 (3) (2010) 249–258.
[150] B. Kouchunas, D. Jabaay, T. Downar, B.S. Collins, S.G. Stimpson, A.T. Godfrey, K.S. Kim, J.C. Gehin, S. Palmtag, F. Franceschini, Validation and Application of the 3D Neutron Transport MPACT within CASL VERA-CS, in: International Topical Meeting on Nuclear Reactor Thermal Hydraulics, NURETH 2015.
[151] Simcenter STAR-CCM+, visited Apr. 9, 2021, https://www.plm.automation.siemens.com/global/en/products/simcenter/STAR-CCM.html.
[152] Extended Storage Collaboration Program (ESCP), EPRI report 1022914, 2011
[153] Extended Storage Collaboration Program International Subcommittee Report, EPRI report 10264812012
[154] Behaviour of Spent Power Reactor Fuel During Storage, TECDOC Series, International Atomic Energy Agency, Vienna, 2019. number 1862
[155] SPAR IV, IAEA, visited Apr. 9, 2021, https://www.iaea.org/projects/crp/t13016.
[156] Demonstrating Performance of Spent Fuel and Related Storage System Components During Very Long Term Storage, TECDOC Series, International Atomic Energy Agency, Vienna, 2019. number 1878